Transportation Research Part C 128 (2021) 103157

Contents lists available at ScienceDirect

Transportation Research Part C

journal homepage: www.elsevier.com/locate/trc

# Modeling, estimation, and control in large-scale urban road networks with remaining travel distance dynamics☆,☆☆

Isik Ilber Sirmatel [a], Dimitrios Tsitsokas [a], Anastasios Kouvelas [b], Nikolas Geroliminis [a,*]

[a] Urban Transport Systems Laboratory, École Polytechnique Fédérale de Lausanne (EPFL), 1015, Switzerland
[b] Institute for Transport Planning and Systems, Eidgenössische Technische Hochschule Zürich (ETH Zürich), 8093, Switzerland

ARTICLE INFO

*Keywords:*
Macroscopic fundamental diagram
Urban road traffic control
Remaining travel distance dynamics
Model-based parameter estimation
Moving horizon observer
Model predictive control

ABSTRACT

City-scale control of urban road traffic poses a challenging problem. Dynamical models based on the macroscopic fundamental diagram (MFD) enable development of model predictive perimeter control methods for large-scale urban networks, representing an advanced control solution carrying substantial potential for field implementation. In this paper we develop a multi-region approximation of the trip-based model, which describes in more details the trip length characteristics compared to existing accumulation-based models. The proposed M-model includes effects of the total remaining travel distance on the transfer flows driving the vehicle accumulation dynamics, potentially yielding improved accuracy over the standard production-over-trip length approximation of the outflow MFD considered in many works on MFD-based modeling and control. We explain that to properly perform perimeter control, boundary queue dynamics have to be integrated. Furthermore, model-based parameter estimation (MBPE), nonlinear moving horizon observer (MHO), and model predictive control (MPC) formulations for the proposed models are presented, forming an integrated traffic control framework. Microsimulation-based case studies, considering an urban network with 1500 links, where the model parameters obtained by MBPE method are used in MHO and MPC design, demonstrate the efficient operation of the proposed framework.

## 1. Introduction

Dynamical modeling, estimation, and control of city-scale urban road networks present considerable challenges. Large size of the systems, inadequate infrastructure and coordination, spatiotemporal propagation of congestion, and interaction between the traffic control system and driver decisions contribute to the difficulties involved when building accurate models and control schemes for urban networks. Considering severe model uncertainty, difficulty of instrumentation, and excessive computational burden associated with detailed link-level modeling and control methods, such traffic management approaches appear to be practically inefficient under congested conditions. As an alternative to these link-level approaches, network-level methods employing perimeter control (i.e., control with actuation over a set of traffic lights on the perimeter between two neighborhood-sized areas) receive increasing attention

☆ 24th International Symposium on Transportation and Traffic Theory. ☆☆ This article belongs to the Virtual Special Issue on IG005584: VSI: ISTTT24.

* Corresponding author.
*E-mail address:* nikolas.geroliminis@epfl.ch (N. Geroliminis).

https://doi.org/10.1016/j.trc.2021.103157
Received 29 December 2020; Received in revised form 8 April 2021; Accepted 11 April 2021
Available online 19 May 2021

as practicable approaches for city-wide traffic control. Employing aggregated modeling and control approaches using only a small subset of all intersections as actuators, the perimeter control method shows substantial promise in alleviating congestion and improving mobility in large-scale urban networks.

Macroscopic fundamental diagram (MFD) of urban traffic emerged as the primary modeling tool enabling development of aggregated modeling and control approaches for large-scale traffic dynamics. An urban region with roughly homogeneous accumulation (i.e., small spatial link density heterogeneity) can be modeled using the MFD, which provides a unimodal, low-scatter, and demand-insensitive relationship between accumulation and trip completion flow. MFD as a concept was first proposed in Godfrey (1969), revisited by Mahmassani et al. (1984) and Daganzo (2007), while it was experimentally proven to exist for urban areas in Geroliminis and Daganzo (2008).

Although a powerful modeling tool, MFD has also its challenges that might undermine its accuracy in expressing urban traffic dynamics: (a) heterogeneous distribution of accumulation, and (b) hysteresis phenomena (see Buisson and Ladier, 2009; Geroliminis and Sun, 2011b; Geroliminis and Sun, 2011a; Saberi and Mahmassani, 2012). Despite its shortcomings, MFD substantially reduces traffic models complexity by avoiding the need for considering the densities of individual network links, which are in the order of thousands for city-scale systems. Appearing thus as an efficient modeling tool for expressing aggregated dynamics of urban traffic, MFD enables the design of model-based control methods for network-level road traffic management.

The idea of network-level traffic control with an MFD-based model was originally proposed by Daganzo (2007) for a single region, where the objective was to operate a region (experiencing high demands for trips) close to capacity, by regulating the inflow at its perimeter, similar to on-ramp metering (or gating). The work first proposes a steady-state approximation to establish the relation between regional outflow (i.e. trip completion rate) and accumulation, which is then used to derive an optimal control strategy in the case of a single congested urban region. Since the first works on MFD-based perimeter control by Keyvan-Ekbatani et al. (2012) and Geroliminis et al. (2013), numerous MFD-based modeling and control methods have been developed for multi-region urban networks (Haddad and Geroliminis, 2012; Aboudolas and Geroliminis, 2013; Kouvelas et al., 2017), alongside approaches using optimal control (Haddad, 2017b; Haddad, 2017a; Aalipour et al., 2019), robust control (Haddad and Shraiber, 2014; Zhong et al., 2018; Mohajerpoor et al., 2020), model-based (Haddad and Mirkin, 2016; Haddad and Mirkin, 2017; Haddad and Zheng, 2020) and model-free adaptive control (Lei et al., 2020; Ren et al., 2020), control via vehicle routing (Ding et al., 2017; Menelaou et al., 2017), cyberattack-resilient control (Haddad and Mirkin, 2020), demand management (Yildirimoglu and Ramezani, 2020), and reinforcement learning (Su et al., 2020).

Enabled via MFD-based modeling approaches, model-based traffic control design methods also received increasing interest: Nonlinear model predictive control (MPC) for a two-region network actuated with perimeter control (Geroliminis et al., 2013), hybrid MPC with perimeter control and switching signal timing plans (Hajiahmadi et al., 2015), dynamical modeling of heterogeneity and hierarchical control with MPC on the upper level (Ramezani et al., 2015), MPC with MFD-based travel time and delays as performance measures (Csikós et al., 2017), two-level hierarchical MPC with MFD-based and link-level models (Zhou et al., 2017), multimodal MFDs network model-based MPC of city-scale ride-sourcing systems (Ramezani and Nourinejad, 2018), MPC with perimeter control and regional route guidance (Sirmatel and Geroliminis, 2018) and extensions with a path assignment mechanism (Yildirimoglu et al., 2018), combined operation of state estimation and MPC (Sirmatel and Geroliminis, 2019). Detailed literature reviews of MFD-based modeling and control can be found in Sirmatel and Geroliminis (2019) and Haddad and Zheng (2020).

Further extensions to MFD-based modeling were also proposed to obtain more detailed models considering heterogeneity effects (Ramezani et al., 2015), boundary queues (Haddad, 2017b; Ni and Cassidy, 2019) and dynamic user equilibrium (Guo and Ban, 2020; Ingole et al., 2020). This paper aims to investigate potential advantages that could be obtained by freeing the standard MFD-based dynamical models from the steady-state approximation associated with using an outflow MFD by the production-over-trip length approach.

When Daganzo (2007) re-introduced these diagrams, he associated them with the concept of network exit function (NEF), thereby highlighting their potential for regional traffic flow management. A NEF is a function expressing the outflow of the zone, i.e. trip completion rate. While outflow is difficult to be measured (unless numerous vehicles are equipped with tracking devices), network production (veh-km traveled per unit time) can be estimated using conventional methods (e.g., loop detectors data) if one assumes that outflow $O$ and production $P$ are linearly related with the average trip length $l$ of a region, i.e., $O = P/l$. We will refer to this specific NEF as the outflow MFD or PL model, while the relations between accumulation and speed (resp. production) will be referred to as speed (resp. production) MFD.

Recently, several authors introduced an alternative description of congestion dynamics, based on the speed MFD but avoiding the steady state approximation (Arnott, 2013; Fosgerau, 2015; Daganzo and Lehe, 2015; Lamotte and Geroliminis, 2018; Jin, 2020), the so-called trip based model (i.e., TB model). This was mainly related to studying the departure time choice problem at the city scale. Trip-based model is computationally more demanding than PL model and may cause intractability; also, it cannot be written in a compact ODE form. Yet, it also provides a sounder treatment of propagation phenomena, avoiding some artifacts associated with PL model, such as the temporary reduction of experienced travel time that can follow a demand surge (see Lamotte and Geroliminis, 2016). A recent paper by Mariotte et al. (2017) analyses some of these issues, but focuses primarily on the consequences of a non-stationary inflow with homogeneous trip length. Nevertheless, such models require full knowledge of the trip length distributions, and, due to the complex dynamics, would potentially cause the numerical optimal control methods based on such models to suffer from problems associated with a high dimensional state.

Lamotte et al. (2018) introduced a third type of NEF for single-region (i.e., the so-called M-model), which reproduces particularly well the behavior of the trip-based model at a much lower computational cost. This is achieved by keeping track of the average remaining distance to be traveled. By comparison, trip-based model keeps track of the distance remaining to be traveled by each

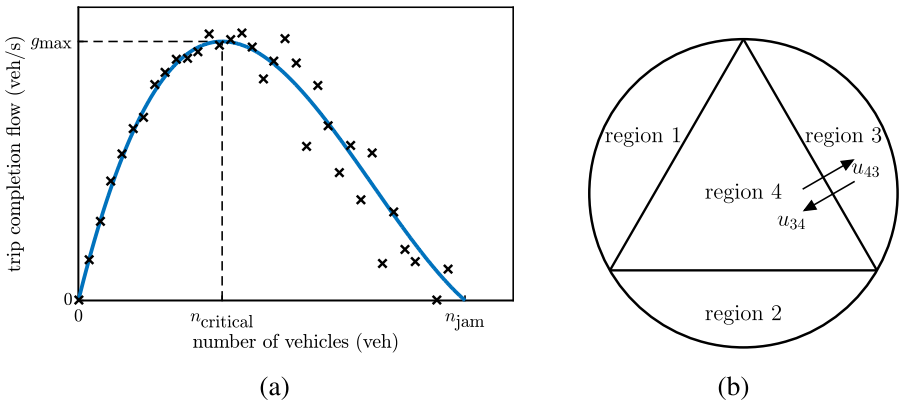


**Fig. 1.** (a) A well-defined outflow macroscopic fundamental diagram. (b) A four region network without route choice.

individual user, while PL model does not keep any record of traveled distance. Such a model offers valuable intuition and represents an attractive trade-off for control applications. The same references showed that all three models (i.e., TB, PL and M) are equivalent in the steady state or when trip length follows an exponential distribution, but this might not be a realistic assumption; nevertheless, the M-model, even if it makes physical sense, has never been tested against real or simulated data. This paper provides contributions both in MFD modeling and multi-region perimeter control on the following directions: (i) modeling heterogeneously congested urban networks with multi-region M-model, (ii) formulating a system identification problem for computing unknown model parameters from historical traffic data, (iii) using the obtained model parameters in model-based observer and control design for improving mobility in urban networks. We utilize both a toy network and a detailed and calibrated micro-simulation model of Barcelona in Spain to provide numerical results.

## 2. MFD-based modeling

### 2.1. A review of modeling with production-over-trip length approximation

Consider a city-scale road traffic network, consisting possibly of hundreds of links and intersections, with heterogeneous distribution of accumulation (i.e., number of vehicles) on its links. Using the macroscopic fundamental diagram (MFD) of urban traffic, it is possible to express the rate of vehicle-meters traveled in a region as a function of region accumulation. Clustering algorithms developed for such large-scale networks (see, e.g., Saeedmanesh and Geroliminis (2016)) can be used to partition the network into regions (i.e., a set of links) to obtain low intraregional accumulation heterogeneity. Empirical results indicate that MFD can be approximated by an asymmetric unimodal curve skewed to the right (Geroliminis and Daganzo, 2008). MFD-based models require the outflow MFD to express interregional vehicle transfer and exit flows, which is usually obtained by approximating the outflow MFD by the production-over-trip length approach formulated as

$$o_i(n_i(t)) = \frac{p_i(n_i(t))}{l_i} = \frac{n_i(t) \cdot v_i(n_i(t))}{l_i}, \tag{1}$$

where $t \in \mathbb{R}$ is the real time, $o_i(n_i(t))$ (veh/s) is the trip completion flow of the region as expressed by the outflow MFD (i.e., rate of vehicles exiting traffic), $n_i$ (veh) is the accumulation in region $i, p_i(n_i(t))$ (veh.m/s) is the production MFD (i.e., rate of vehicle-meters traveled), $l_i$ (m) is the average trip length for vehicles in region $i$ (until exiting their current region $i$), whereas $v_i(n_i(t))$ (m/s) is the speed MFD expressing space-mean speed of region $i$.

Given a network $\mathcal{R}$ consisting of a set of $R$ regions ($\mathcal{R} = \{1,2,\ldots,R\}$) (see, e.g., fig. 1(b)), each with a well-defined MFD, aggregated dynamical models of large-scale road traffic networks can be developed based on inter-regional traffic flows as the following vehicle conservation equations (Ramezani et al., 2015):

$$\dot{n}_{ii}(t) = q_{ii}(t) - o_{ii}(t) + \sum_{h \in \mathcal{N}_i} u_{hi}(t) o_{hii}(t) \tag{2a}$$

$$\dot{n}_{ij}(t) = q_{ij}(t) - \sum_{h \in \mathcal{N}_i} u_{ih}(t) o_{ihj}(t) + \sum_{h \in \mathcal{N}_i; h \neq j} u_{hi}(t) o_{hij}(t), \tag{2b}$$

where $n_{ii}(t)$ (veh) and $n_{ij}(t)$ (veh) are state variables expressing the accumulation in region $i$ with destination region $i$ and $j$, respectively, with $n_i(t) = \sum_{j=1}^{R} n_{ij}(t), q_{ii}(t)$ (veh/s) and $q_{ij}(t)$ (veh/s) are disturbances expressing the rate of vehicles appearing in region $i$ demanding trips to destination region $i$ and $j$, respectively, $u_{ih}(t) \in [\underline{u}, \overline{u}]$ (with $0 \leqslant \underline{u} < \overline{u} \leqslant 1$) are perimeter control inputs between each pair of adjacent regions $i$ and $h$, expressing actions of perimeter control actuators (with $h \in \mathcal{N}_i$; where $\mathcal{N}_i$ is the set of regions adjacent

to $i$) that can adjust vehicle flows transferring between the regions, $o_{ihj}(t)$ (veh/s) is the vehicle flow transferring from $i$ to $h$ with destination $j$:

$$o_{ihj}(t) \triangleq \theta_{ihj}(t)\frac{n_{ij}(t)}{n_i(t)}o_i(n_i(t)), \tag{3}$$

where $\theta_{ihj}(t) \in [0,1]$ is the route choice term expressing, for the vehicles exiting region $i$ with destination $j$, the ratio that is transferring to region $h$ (with $o_{hii}(t)$ and $o_{hij}(t)$ defined similarly), whereas $o_{ii}(t)$ (veh/s) is the exit (i.e., internal trip completion) flow of region $i$:

$$o_{ii}(t) \triangleq \frac{n_{ii}(t)}{n_i(t)}o_i(n_i(t)). \tag{4}$$

Note that route choice effect can be omitted in modeling if the network topology leads to a single obvious route choice, in which case $\theta_{ihj}(t) = 1$ for all time for only one region $h \in \mathcal{N}_i$ for each $i$-$j$ pair (with $j \neq i$). For example, for the network depicted in fig. 1(b), $\theta_{4hj}(t) = 1$ if $h = j$, and $\theta_{4hj}(t) = 0$ otherwise. The focus of this paper is on those networks where route choice can be omitted (see Sirmatel and Geroliminis, 2018 for a study where it is included).

### 2.2. Trip based models and approximations

Having revisited production-over-trip length approximation based dynamical models commonly encountered in the MFD literature in the previous section, in this section we derive the foundations of the M model (based on the work in Lamotte et al. (2018)), and extend it to develop a multi-region dynamical M model.

All MFD type dynamic models rely on the conservation equation

$$\dot{n}(t) = I(t) - O(t), \tag{5}$$

where $n(t)$ denotes the accumulation of vehicles inside the zone, $\dot{n}$ its time derivative, $O(t)$ the outflow rate and $I(t)$ the inflow rate (note that trips may start either inside the zone, or by crossing the perimeter). While the inflow rate is often exogenous, outflow rate is estimated via a network exit function (NEF). Denoting the average trip length as $l$, outflow MFD can be derived as a simple expression for this outflow:

$$O(t) = \frac{n(t)\cdot v(t)}{l} = \frac{P(t)}{l}. \tag{6}$$

Daganzo (2007) postulated that this result still holds approximately as long as the production MFD exists and inflow varies slowly enough, so that $O(t)$ can be approximated as $O_{\mathrm{PL}}(t) = O(n(t)) = P(n(t))/l$ (hence the appellation "PL model"). Validity of this assumption was empirically observed by Geroliminis and Daganzo (2008), who observed using both loop detector and taxi data that the ratio of production over trip completion rate remained approximately constant over time for the city of Yokohama, Japan.

Trip-based model (TB) builds on the existence of a speed MFD $v(n(t))$, and derives outflow without requiring the PL model steady state assumption. An intuitive way to introduce the trip based model analytically for a single region is to consider that a user with trip length $l_0$ that enters the system at time $t_0$ should exit after traveling distance $l_0$ with travel time $\tau_0$, satisfying

$$\int_{t_0}^{t_0+\tau_0} v(n(\tau))d\tau = l_0. \tag{7}$$

Among the users that entered the network at time $s$, the proportion that is still in the network at time $t > s$ is given by $1 - F_{\mathrm{cdf}}(\int_s^t v(n(\tau))d\tau)$, where $F_{\mathrm{cdf}}(\cdot)$ is the cumulative distribution function (cdf) of trip length, corresponding to the trip-generating process, with the corresponding probability density function (pdf) denoted by $f$. While in the general case $F_{\mathrm{cdf}}(\cdot)$ might be time dependent (e.g., due to rerouting and longer paths under congestion), it can be considered constant (as for example empirical data from Yokohama have shown in Geroliminis and Daganzo (2008)). Assuming that flow $I(s)$ entering the zone is known for all times $s < t$, and that $I(s) = 0$ for all times $s < 0$, the accumulation at time $t$ is

$$n(t) = \int_0^t I(s)\left(1 - F_{\mathrm{cdf}}\left(\int_s^t v(n(\tau))d\tau\right)\right)ds. \tag{8}$$

By differentiating the above equation, we obtain an expression that has the same form as eq 5, but where the outflow is described by:

$$O_{TB}(t) = v(n(t))\int_0^t I(s)f\left(\int_s^t v(n(\tau))d\tau\right)ds. \tag{9}$$

While this expression is difficult to solve analytically, it can be easily implemented in an event- and agent-based simulation (see Section 4.2 of Lamotte et al. (2018)). Lamotte et al. (2018) also define an approximation of the trip-based model, named M model with an additional state variable $m(t)$ representing the total remaining distance to be travelled by all vehicles currently in the network. The dynamics of $m$ state can be expressed as:

$$\dot{m}(t) = I(t)l - n(t)v(n(t)), \tag{10}$$

simply meaning that the rate of the total remaining distance increases by the generating demand multiplied by the average trip length and decreases by the current production rate $n(t)v(n(t))$.

By considering now multiple regions with a speed MFD $v_i(n_i(t))$ for each region $i$ (with $i \in \mathcal{R}$), i.e., $v_i(n_i(t)) = p_i(n_i(t))/n_i(t)$, the outflow MFD $o_i(n_i(t))$ can be reformulated to account for variations in the remaining distance to be traveled as follows, i.e., with the M-model approach (building on the single region model of Lamotte et al. (2018)):

$$o_i(n_i(t), m_i(t)) = \frac{n_i(t) \cdot v_i(n_i(t))}{l_i}\left(1 - \alpha_i \cdot \left(\frac{m_i(t)}{n_i(t) \cdot l_i^*} - 1\right)\right), \tag{11}$$

where $\alpha_i \geqslant 0$ is a model parameter expressing the sensitivity of outflow $o_i(n_i(t), m_i(t))$ in relation to variations in the remaining distance to be traveled, $m_i(t)$ (veh.m) is the total remaining distance to be traveled by all vehicles in region $i$, whereas $l_i^*$ is the average remaining distance to be traveled in steady state for vehicles in region $i$ (until exiting their current region $i$) and $l_i$ is the average trip length of vehicles in region $i$ (according to the definition of the $f$ distribution defined above). The ratio $m_i(t)/n_i(t)$ expresses the average remaining distance to be travelled by vehicles currently in region $i$, which might be different than the steady state value $l_i^*$. Thus, the dimensionless quantity inside the parenthesis multiplied by $\alpha_i$ can be positive or negative.

In steady state, the average distance remaining to be traveled is simply given by $l^* = \int_0^{+\infty} g(\delta)\frac{\delta}{2}d\delta$, where $g$ is the pdf of the trip length distribution among all users present in a snapshot (note that $g$ is different than $f$). Since users remain in the network for a duration proportional to their trip length, $g(\delta)$ is proportional to $f(\delta)\delta$. Imposing that $\int_0^{+\infty} g(\delta)d\delta = 1$ implies that $g(\delta) = f(\delta)\frac{\delta}{l}$. Thus:

$$l^* = \int_0^{+\infty} g(\delta)\frac{\delta}{2}d\delta = \int_0^{+\infty} f(\delta)\frac{\delta^2}{2l}d\delta = \frac{l^2 + \sigma^2}{2l}. \tag{12}$$

We are now ready to extend the M-model in the case of multi-region systems governed by MFD dynamics. For writing the urban dynamics with $n_{ij}(t)$ as state variables, we need the transfer flow terms $o_{ihj}(t)$, which we write in the following form considering also the remaining distance to be traveled:

$$o_{ihj}^m(t) = \theta_{ihj}(t)\frac{n_{ij}(t) \cdot v_i(n_i(t))}{l_{ij}}\left(1 - \alpha_{ij} \cdot \left(\frac{m_{ij}(t)}{n_{ij}(t) \cdot l_{ij}^*} - 1\right)\right), \tag{13}$$

where $l_{ij}$ (m) is the average trip length for vehicles in region $i$ destined to region $j$ (until exiting their current region $i$), $\alpha_{ij} \geqslant 0$ is a model parameter expressing how sensitive the transfer flow $o_{ihj}^m(t)$ is to variations in the remaining distance to be traveled, $m_{ij}(t)$ (veh.m) is the total remaining distance to be traveled by vehicles in region $i$ destined to region $j$, whereas $l_{ij}^*$ is the average remaining distance to be traveled in steady state for vehicles in region $i$ destined to region $j$ (until exiting their current region $i$). Note that, While for a PL model steady state satisfies the conditions $\dot{n}(t) = 0$, for an M model the steady state conditions should satisfy $\dot{n}(t) = 0$ and $\dot{m}(t) = 0$. The exit flow $o_{ii}^m(t)$ can be formulated similarly as follows:

$$o_{ii}^m(t) = \frac{n_{ii}(t) \cdot v_i(n_i(t))}{l_{ii}}\left(1 - \alpha_{ii} \cdot \left(\frac{m_{ii}(t)}{n_{ii}(t) \cdot l_{ii}^*} - 1\right)\right), \tag{14}$$

with the parameters and variables defined analogously to the $o_{ihj}^m(t)$ case.

Extension of a single- to multi-region M-model cannot be made by simply following the same logic as in PL models: To yield consistency between the $m_{ij}(t)$ and $n_{ij}(t)$ states, we need to account for the fact that not all vehicles ending their trips inside a region (and are destined to another region, i.e., those that are expressed by the transfer flow terms $o_{ihj}^m(t)$) might necessarily immediately transfer to another region, due to the restrictions by the perimeter control inputs $u_{ih}(t)$, getting delayed instead at the queues on the boundary between regions. From the perspective of $m_{ij}(t)$ dynamics, these vehicles ended their trips and thus get discharged from $m_{ij}(t)$ state (since they do not have any remaining distance to travel anymore) with the production term $n_{ij}(t)v_i(n_i(t))$. However, from the perspective of $n_{ij}(t)$ dynamics, since they did not actually transfer to another region, they are not discharged from $n_{ij}(t)$ state, and thus, although they finished their trips, they are still considered a part of the traffic inside the model (i.e., they affect the average speed value as modeled by the speed MFD $v_i(n_i(t))$, since $n_i(t) \triangleq \sum_{j\in\mathcal{R}} n_{ij}(t)$). This discrepancy can be resolved by adding boundary queue dynamics to the model, which will allow us to differentiate between vehicles inside region $i$ that are still traveling and those that finished their trips. Boundary queue dynamics for MFD PL models were first introduced by Haddad (2017b), while an expanded formulation with dynamic boundaries was proposed by Ni and Cassidy (2019). We can formulate the boundary queue dynamics as follows:

$$\dot{n}_{ihj}^q(t) = o_{ij}^m(t) - u_{ih}(t)o_{ihj}^q(t), \tag{15}$$

where $n_{ihj}^q(t)$ (veh) is the accumulation state expressing the number of vehicles inside region $i$, destined to $j$, queuing at the boundary for transferring to $h$ (with $h \in \mathcal{N}_i$), whereas $o_{ihj}^q(t)$ (veh/s) is the transfer flow (from the queue at the boundary of regions $i$ and $h$) of vehicles in $i$ transferring to $h$ with destination $j$, which can be expressed as follows:

$$o^q_{ihj}(t) = \frac{n^q_{ihj}(t)}{n^q_{ih}(t)} o^q_{ih}(n^q_{ih}(t)), \tag{16}$$

where $n^q_{ih}(t)$ (veh) is the total accumulation at the $i$-$h$ boundary queue (with $n^q_{ih}(t) \triangleq \sum_{j\in\mathcal{R}} n^q_{ihj}(t)$), whereas $o^q_{ih}(\cdot)$ (veh/s) is the outflow of the $i$-$h$ boundary queue, which can be modeled via a fundamental diagram in the form of a third degree polynomial:

$$o^q_{ih}(n^q_{ih}(t)) = a_{ih}(n^q_{ih}(t))^3 + b_{ih}(n^q_{ih}(t))^2 + c_{ih} n^q_{ih}(t), \tag{17}$$

where $a_{ih}, b_{ih}, c_{ih}$ are the parameters of the fundamental diagram.

Using the aforementioned definitions of transfer flows, dynamics of accumulations can be formulated as follows:

$$\dot{n}_{ii}(t) = q_{ii}(t) + \sum_{h\in\mathcal{N}_i} u_{hi}(t) o^q_{hii}(t) - o^m_{ii}(t) \tag{18a}$$

$$\dot{n}_{ij}(t) = q_{ij}(t) + \sum_{h\in\mathcal{N}_i; h\neq j} u_{hi}(t) o^q_{hij}(t) - \sum_{h\in\mathcal{N}_i} o^m_{ihj}(t). \tag{18b}$$

Moreover, we can write the dynamics of total remaining distance to be traveled $m_{ij}(t)$:

$$\dot{m}_{ii}(t) = \left( q_{ii}(t) + \sum_{h\in\mathcal{N}_i} u_{hi}(t) o^q_{hii}(t) \right) l_{ii} - n_{ii}(t) v_i(n_i(t)) \tag{19a}$$

$$\dot{m}_{ij}(t) = \left( q_{ij}(t) + \sum_{h\in\mathcal{N}_i; h\neq j} u_{hi}(t) o^q_{hij}(t) \right) l_{ij} - n_{ij}(t) v_i(n_i(t)), \tag{19b}$$

which can be intuitively understood as follows: With each vehicle appearing in the region (i.e., either with inflow demand $q_{ii}(t)$-$q_{ij}(t)$ or via transfer flows $u_{hi}(t)o^q_{hii}(t)$-$u_{hi}(t)o^q_{hij}(t)$ from the boundary queues), the total remaining distance to be traveled $m_{ij}(t)$ increases by the amount each vehicle needs to travel until finishing its trip inside the current region (i.e., by $l_{ij}$ on average), while it decreases by the rate of vehicle-meters traveled, i.e., the production $n_{ij}(t)v_i(n_i(t))$.

A significant challenge that requires further investigation is how the size of boundary queue region influences the dynamics of M-model. If this region becomes very congested, then propagation of congestion within the main region of the city (represented by M-model) can affect the distribution of remaining distance to be traveled and make the M-model inaccurate. We can handle this in two different ways: (i) By adding constraints in the number of vehicles that a boundary queue region can contain (similar to ramp metering policies with max-queue constraints at the on-ramps; see, e.g., Papamichail and Papageorgiou (2010)) (ii) by varying the size of the boundary region. While Ni and Cassidy (2019) have modeled time-varying cordon queues by considering that they exhibit jam densities all times, Variational Theory (VT) applications for MFDs have shown that as the outflow of these regions is non-zero, average density might vary. While queued vehicles variables have been estimated implicitly in Ni and Cassidy (2019), our intention is to measure these variables in the boundary queue regions.

## 3. Identification and control

Discretizing the dynamics given in Eqs. (15), (18) and (19) in time with a sampling time $T$, and writing them in compact form, we end up with the following vector nonlinear difference equation:

$$x(k+1) = F(x(k), q(k), u(k), p), \tag{20}$$

where $k \in \mathbb{N}_0$ is the time step of sampled real time (i.e., $t(k) = T \cdot k$), $x(k) \in \mathbb{R}^{n_x}$ (state) is a vector containing all M-model state variables (i.e., accumulations $n_{ij}(k)$, boundary queue accumulations $n^q_{ihj}(k)$, and total remaining distance to be traveled $m_{ij}(k)$), $q(k) \in \mathbb{R}^{n_q}$ (measured disturbance) is a vector containing all inflow demands $q_{ij}(k), u(k) \in \mathbb{R}^{n_u}$ (control input) is a vector containing all perimeter control input terms $u_{ih}(k)$, whereas $p \in \mathbb{R}^{n_p}$ (parameters) is a vector containing all terms defined as constant model parameters. These parameters are the MFD parameters $a_i, b_i$, and $c_i$, together with the M-model related parameters $\alpha_{ij}, l^*_{ij}$, and $l_{ij}$.

Assuming additive measurement noise, the measurement equation for the case where full state measurements are available can be formulated as follows:

$$x^{\mathrm{m}}(k) = x(k) + v^{\mathrm{m}}(k), \tag{21}$$

where $x^{\mathrm{m}}(k) \in \mathbb{R}^{n_x}$ is the full state measurement, $v^{\mathrm{m}}(k) \in \mathbb{R}^{n_y}$ the full state measurement noise vector (with $v^{\mathrm{m}}(k) \sim \mathcal{N}(0, \Sigma_{v^{\mathrm{m}}})$), whereas for the case where $m_{ij}(k)$ cannot be measured we denote the partial measurements as $y(k)$ and formulate the measurement equation as follows:

$$y(k) = h(x(k)) + v(k) \tag{22}$$

where $y(k) \in \mathbb{R}^{n_y}$ is the vector of partial measurements, $v(k) \in \mathbb{R}^{n_v}$ the measurement noise vector (with $v(k) \sim \mathcal{N}(0, \Sigma_v)$), while $h(\cdot)$ is the function expressing the measurement equations in the following form:

$$h(x(k)) = \begin{bmatrix} n(k) \\ n^q(k) \end{bmatrix}, \tag{23}$$

where $n(k)$ is the vector of accumulations $n_{ij}(k)$ while $n^q(k)$ is the vector of boundary queue accumulations $n^q_{ihj}(k)$.

### 3.1. Model-based parameter estimation

In system identification the concern is to extract mathematical models of dynamical systems from data. Here we consider using a particular class of system identification methods termed model-based parameter estimation (MBPE), which involves formulating an optimization problem using the dynamical model, the parameters of which are to be estimated (see Bock et al., 2013 for details).

For MBPE using the M-model, we propose the following formulation based on the least-squares prediction error method of Ljung (2002) (applied to MFD-based models first in Sirmatel and Geroliminis (2020)):

$$\text{minimize}_p \quad \sum_{\kappa=0}^{N_{\text{pe}}} \| x^{\text{m}}(\kappa) - x_\kappa \|_R^2 \tag{24}$$

$$\text{subject to} \quad \underline{p} \leqslant p \leqslant \overline{p} \tag{25}$$

$$\text{for } \kappa = 0, \ldots, N_{\text{pe}} - 1: \tag{26}$$

$$x_{\kappa+1} = F(x^{\text{m}}(\kappa), q(\kappa), u(\kappa), p) \tag{27}$$

where $p$ is the vector of model parameters to be estimated, $\kappa$ is the time interval index of MBPE, $N_{\text{pe}}$ is the MBPE experiment horizon, $R$ is an approximation of the inverse covariance matrix $\Sigma_{v^{\text{m}}}^{-1}$ of the full state measurement noise $v^{\text{m}}$, $\underline{p}$ and $\overline{p}$ are known lower and upper bounds on the parameters (possibly obtained from an analysis on historical data and/or by physical intuition), respectively, $x^{\text{m}}(\kappa)$, $q(\kappa)$, and $u(\kappa)$ are trajectories of full state measurements, inflow demands, and control inputs, respectively, recorded at discrete intervals $\kappa = 0, \ldots, N_{\text{pe}}$, whereas $x_\kappa$ is a variable representing the state $x(k)$ internal to MBPE.

### 3.2. Moving horizon observer

In practice it is expected to be difficult to measure the total remaining distance to be traveled states $m_{ij}(k)$ in real time, complicating the use of M-model for model-based traffic control. Here we propose using an observer to reconstruct traffic states from incomplete measurements in real-time. For a dynamical system in the form given in eq. 20 together with measurement Eq. (22), the problem of observing system state, roughly stated, corresponds to obtaining an observation $\widehat{x}(k)$ which is similar to the actual state $x(k)$, given recent measurements $y(k)$, measured disturbances $q(k)$, and inputs $u(k)$ (see Besançon, 2007 for details).

Notice that the state observation problem is different than the more general state estimation problem, where the former involves no uncertainty and corresponds simply to reconstructing the state from incomplete measurements (i.e., $h(x(k)) \neq x(k)$), while the latter involves obtaining state estimates considering uncertainty and also state reconstruction if necessary (see Sirmatel and Geroliminis, 2019 for a study on MFD-based state estimation using the PL model). Although it might be possible to use state observers for cases with low to moderate uncertainty, using state estimators that incorporate uncertainty in their formulation may be necessary for cases where observers have poor performance. Design of state estimation schemes for the M-model can be considered in future work.

Following the methodology developed in Michalska and Mayne (1995), we propose a nonlinear moving horizon observer (MHO), which involves reconstructing the state trajectory on a moving time horizon extending a fixed length into the past using associated measurements and control inputs by solving the following optimization problem:

$$\text{minimize}_{x_\kappa} \quad \sum_{\kappa=-N_{\text{o}}}^{0} \| y(k+\kappa) - h(x_\kappa) \|^2 \tag{28}$$

$$\text{subject to} \quad \text{for } \kappa = -N_{\text{o}}, \ldots, 0: \tag{29}$$

$$0 \leqslant x_\kappa \leqslant \overline{x} \tag{30}$$

$$\text{for } \kappa = -N_{\text{o}}, \ldots, -1: \tag{31}$$

$$x_{\kappa+1} = F(x_\kappa, q(k+\kappa), u(k+\kappa), \widehat{p}) \tag{32}$$

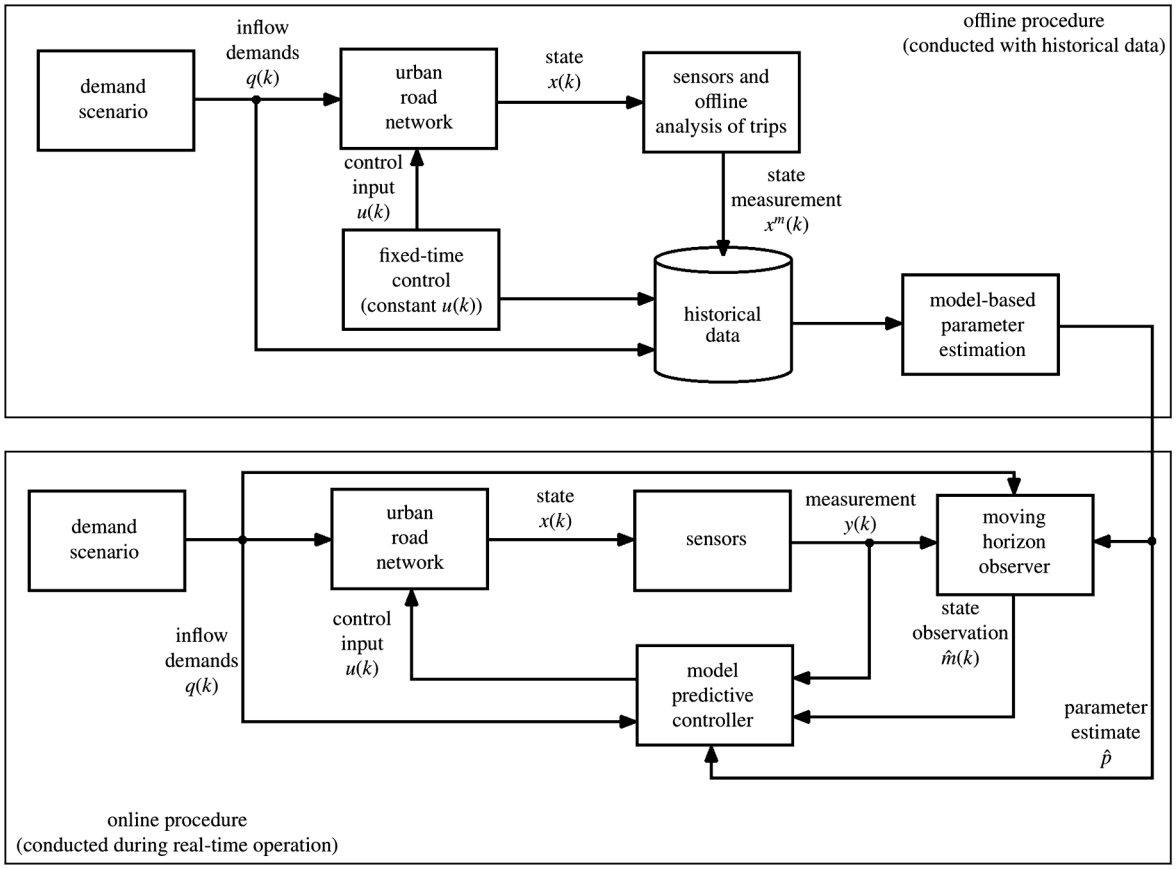


**Fig. 2.** Block diagram showing the information flow between procedures and components of the traffic management system.

where $\kappa$ is the MHO time interval index, $k$ the current time step, $N_o$ the observation horizon, $x_\kappa$ the state vector internal to the MHO, $y(k), q(k)$, and $u(k)$ are measurements, inflow demands, and perimeter control inputs recorded at time step $k$, respectively, $\bar{x}$ a known upper bound on the state (which can be obtained by analysing usual values of $x(k)$ from historical data and choosing reasonable upper bounds on them), whereas $\hat{p}$ is the parameter estimate obtained via MBPE as the solution of (24).

To be able to formulate an MHO problem, we need to express a penalization of the mismatch between the actual and simulated measurements (i.e., $y$ and $h(x)$ in eq. 28). The usual way of doing this, also highly preferable from the optimization point of view as it leads to a convex quadratic objective function, is to use the $l_2$-norm of the mismatch (as is done here). For the case of moving horizon estimation (where process and measurement noise are explicitly modeled), the objective function has a probabilistic interpretation in the sense that, for example, using the (weighted) $l_2$-norm corresponds to assuming the mismatch (noise) to have Gaussian distribution, with the weighting matrix representing the inverse covariance matrix of the noise. Another possibility is to use the $l_1$-norm of the mismatch, which corresponds to assuming the noise to have Laplace distribution. For the case of MHO, the choice of $l_2$-norm is mainly for convenience (since it is a straightforward norm to use in computations) and for the benefit of optimization algorithms, however it could also be interpreted as considering the mismatch, although not explicitly modeled as one, to be caused by measurement noise with Gaussian distribution (with all elements of the mismatch, i.e., all noise terms of individual sensors, assumed to have the same variance), which is not an unreasonable assumption. The MHO can suffer from deteriorating performance in cases of: a) excessive noise in the measurements, b) noise present in individual sensors having different characteristics with respect to probability, c) substantial plant/model mismatch (i.e., the dynamics $F(\cdot)$ does not represent reality well). In such cases, resorting to explicitly modeling the measurement noise (to represent different noise characteristics of the sensors) and process noise (to take modeling uncertainty into account), via using e.g. moving horizon estimation, is advisable, which we consider as a possible direction for future work.

### 3.3. Model predictive control

The problem of finding the control inputs that minimize total time spent (TTS) for a finite horizon can be formulated as the following economic nonlinear MPC problem (based on the work in Geroliminis et al. (2013)):

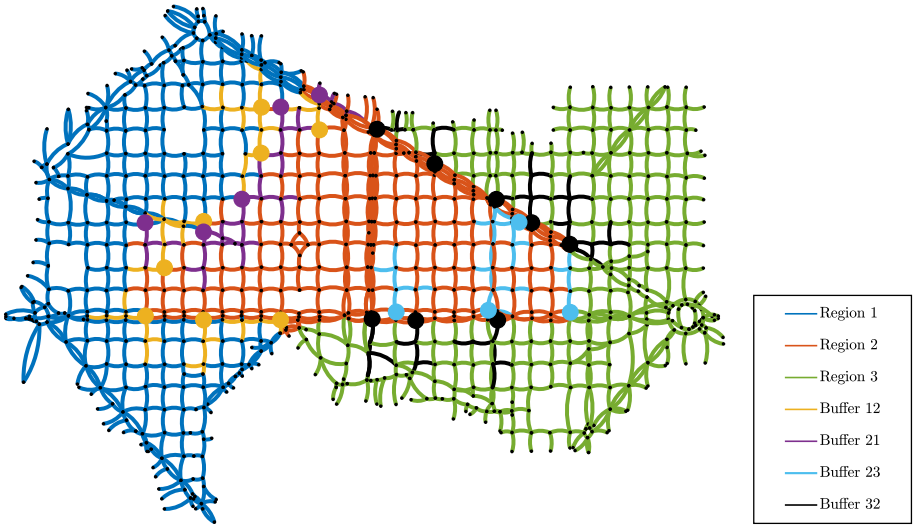


**Fig. 3.** Microscopic (Aimsun) model of the network, with clustering results as links and controlled intersections as circles (intersections belonging to $u_{12}$ in yellow, $u_{21}$ in magenta, $u_{23}$ in cyan, and $u_{32}$ in black). (For interpretation of the references to color in this figure legend, the reader is referred to the web version of this article.)

$$\text{minimize}_{u_\kappa} \quad \sum_{\kappa=1}^{N_c} \mathbf{1}^\top x_\kappa \tag{33}$$

$$\text{subject to} \quad x_0 = \widetilde{x}(k) \tag{34}$$

$$|u_0 - u(\kappa-1)| \leqslant \Delta_u \tag{35}$$

$$\text{for } \kappa = 0, \ldots, N_c - 1: \tag{36}$$

$$x_{\kappa+1} = F(x_\kappa, q(k), u_\kappa, \widehat{p}) \tag{37}$$

$$\underline{u} \leqslant u_\kappa \leqslant \overline{u} \tag{38}$$

$$\text{for } \kappa = 1, \ldots, N_c: \tag{39}$$

$$n_{i,\kappa} \leqslant n_{i,\text{jam}} \quad \forall i \in \mathcal{R}, \tag{40}$$

where $\kappa$ is the MPC time interval index, $k$ the current time step, $N_c$ the prediction horizon, $x_\kappa$ and $u_\kappa$ are the state and control input vectors internal to the MPC, respectively, $\mathbf{1}_{\setminus m}$ is a vector of ones and zeros of appropriate dimension (with $\mathbf{1}^\top x_\kappa$ expressing the sum of accumulation state variables in $x_k$ (i.e., excluding the $m_{ij}$ states), which, multiplied by the sampling time $T$, yields an objective function describing the TTS), $\widetilde{x}(k)$ denotes the information on state $x(k)$ available at current time step $k$ (a combination of the measurements on $n(k)$ and $n^q(k)$, together with the observation on $m(k)$ obtained via MHO as the solution of (28)), $\Delta_u$ is the rate limiting parameter on control inputs, $\underline{u}$ and $\overline{u}$ are the control input constraints, whereas $n_{i,\kappa}$ denotes the total accumulation in region $i$.

Operation of the traffic management system consisting of the proposed MBPE, MHO, and MPC schemes can be formalized in the form given in algorithm 1, and visually depicted as a block diagram showing the flow of information over system components in fig. 2. For the MBPE, it is assumed that all state variables (i.e., $n_{ij}, n^q_{ij}$, and $m_{ij}$) are recorded as historical data, and thus these are available during the offline procedure where MBPE is conducted to find the parameter estimate $\widehat{p}$. Vehicle trajectory data is used to generate the $m_{ij}$ trajectories that are used for MBPE during the offline procedure, while for $n_{ij}$ and $n^q_{ij}$ (i.e., the accumulations of regions and boundary queues), it is assumed that they are available as measurements, both for MBPE, and as real-time sensor measurements for the online procedure (i.e., for MHO and MPC). Although assuming $n_{ij}$ and $n^q_{ij}$ are available as real-time measurements is not realistic,

linking practical sensor data (such as loop detectors) to macroscopic variables (such as $n_{ij}$) is part of ongoing research, and thus more effort is needed to establish the connection.

**Algorithm 1.** Operation of identification and traffic control.

Offline: Using historical data on state measurements $x^{m}(k)$, solve the MBPE (24) to obtain the parameter estimate $\widehat{p}$.
Online: Initialize operation from $x(0)$ at $k = 0$. Then, at each time step $k$:
1) Given partial state measurements $\{y(k+\kappa)\}_{\kappa=-N_o}^{0}$, inflow demands $\{q(k+\kappa)\}_{\kappa=-N_o}^{-1}$, and control inputs $\{u(k+\kappa)\}_{\kappa=-N_o}^{-1}$, solve the MHO problem (using $\widehat{p}$) (28) to obtain the state observation trajectory $\{\widehat{m}^{*}_{k+\kappa}\}_{\kappa=-N_o}^{0}$.
2) Given the last element $\widehat{m}(k) = \widehat{m}^{*}_{k}$ of the state observation trajectory for the $m(k)$ state, and the measurements on $n(k)$ and $n^{q}(k)$, solve the MPC problem (using $\widehat{p}$) (33) to obtain the control input trajectory $\{u^{*}_{k+\kappa}\}_{\kappa=0}^{N_c}$.
3) Apply the first element $u_k = u^{*}_{k}$ of the control input trajectory to the system.
4) Evolve system state by waiting for the next time step (for real operation) or by simulating the system dynamics via eq. 20 (using $\widehat{p}$).
Repeat steps 1, 2, 3, and 4 for $k \in \mathbb{Z}_{\geqslant 0}$ up to $k_{\text{final}}$.

## 4. Case study and results

### 4.1. Network setup

An urban road network consisting of roughly 1500 links and 600 intersections is replicated as a computer model using the microscopic simulation package Aimsun (see fig. 3). The model represents a portion of the urban network of the city of Barcelona in Spain, covering an area of 12 km$^2$. The network is partitioned into three regions using the optimization-based clustering method of Saeedmanesh and Geroliminis (2016). The direction of the road is represented by the curvature of the links in the graph ( fig. 3), considering counter-clockwise movement of vehicles. Drivers in the simulations are adaptive and vehicles update their routes dynamically based on real-time traffic information and a predefined dynamic traffic assignment strategy. We also introduce some buffer zones between regions, where it is expected that vehicles near the perimeter of the control region will form longer queues compared to the rest of the zone. For the buffer zones we consider links that are up to a distance of 3 links from the traffic lights that are part of the perimeter control strategy (28 in total as can be seen in fig. 3). We consider only the links that are not against the direction of traffic. Based on the control results, the size of the buffer zones ensure that overflows occur rarely to the main MFD regions. As explained in the introduction, these buffers are necessary in M-model so that outflows from regions are estimated properly. Furthermore, fig. 4 shows the distribution of trip length for all vehicles that travelled in the course of the simulation. We also use a toy network with the same representation of 3 regions and 4 buffer zones, where individual vehicles are not simulated but the dynamics are those of eq. 20 with additive noise. The aggregated demand and speed MFDs for the toy network are the same with the micro-simulation model to remain consistent in the paper. Note that the results involve microscopic simulations for the identification study, while the tests with the control system (i.e., MHO and MPC) are done using macroscopic simulations, where the model parameters and demand scenario are extracted from microscopic simulations.

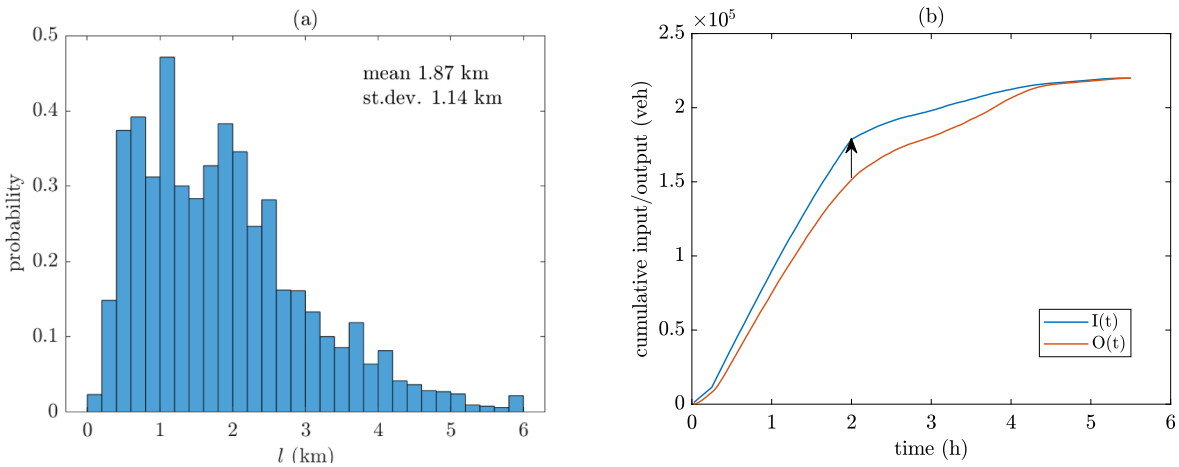


**Fig. 4.** (a) Trip length distribution $f$ of all generating trips in the network; (b) Cumulative input-output diagram for the entire network and simulation time; the arrow indicates the time $t = 2$ hours of maximum accumulation, after which outflow is higher than inflow and the network starts unloading.

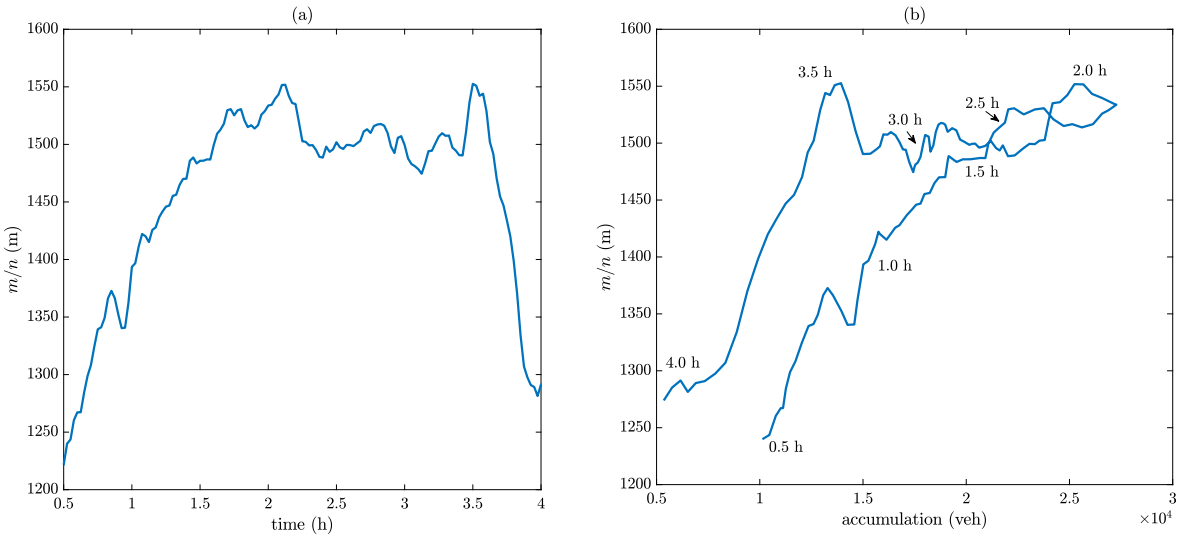


**Fig. 5.** $m/n$ plots: (a) Time series of average remaining distance $m/n$ for the whole network. (b) $m/n$ vs. accumulation for the whole network. Average remaining distance in steady state $l^* = 1.28$ km.

### 4.2. Multi-region M model simulation results

In this section we perform an analysis of individual vehicle trajectories and we investigate how trip length and remaining distance to be travelled are influenced by the network conditions in a realistic scenario of a complex network governed by MFD properties. Note that in the simulation experiment, the last 1 h of generating demand is close to zero, so that the network can clear by the end of the simulation with no remaining circulating vehicles. This can allow the comparison of different control strategies in the next section for scenarios with almost identical total vehicles served during the simulation horizon. During this last period of the simulation, some atypical situation is observed, where a group of few links demonstrate particularly high density (local gridlocks) and strong rerouting. As this is an artifact of the simulation software, this period is excluded from the analysis of trip length distributions. The first 30 min of network warm-up are also excluded.

Remaining distance to be traveled to reach each destination is calculated every 90 s for every vehicle circulating in the network at this time (snapshot). The trip length for each vehicle during its whole trip is also extracted from the dataset. Consequently, we perform the same calculations for a network partitioned as per fig. 3 with 3 regions. Finally, the aforementioned two variables are calculated per region until a vehicle crosses in another region or finishes its trip within this region (in a similar manner as accumulations $n_{ij}$ are calculated).

Fig. 4(a) represents the trip length distribution of all generating trips while Fig. 4(b) represents the cumulative input-output of the entire network including all trips of the simulation. Note that before $t = 2$ hours, generating input is higher than output (trip endings) while the opposite happens after this time. The average remaining distance variation during the simulation horizon is presented in fig. 5. For a given time, this is calculated as the sum of remaining distances of all vehicles currently in the network $m$ divided by the total network accumulation $n$; fig. 5(a) shows the evolution of $m/n$ over time. Note here that $m/n$ is the actual average remaining distance, while $l^*$ is the one in steady state. The difference between $m/n$ and $l^*$ is the main reason that the PL model is not very accurate. Note that if $m/n = l^*$ then Eq. 11 simplifies to the outflow of a PL model (i.e., Eq. 1). Interestingly, there is strong variation across time due to the fact that congestion builds. As inflow is higher than outflow and accumulation increases, the average remaining distance increases. This happens because in fig. 5(a) the number of vehicles with longer trips remain in the network for longer time and are influenced more by congestion. Note that for PL model that has memoryless properties, average remaining distance has to remain constant if trip length distribution is constant. The reason that $m/n$ increases in the onset of congestion is the following. When inflow $I(t)$ is higher than outflow $O(t)$, newly generated trips are entering in the network sampled from the distribution $f$ as defined in Section 2.2. As outflow is smaller, the distribution of remaining distance shifts to the right and its average $m/n$ is expected to increase. The opposite is expected to happen in the offset of congestion, when $O(t) > I(t)$, provided that the snapshot distribution $g$ of trip length is relatively constant. In this case, one can notice that while accumulation starts decreasing after about 2 h and outflow is higher than inflow, $m/n$ does not change significantly between 2 and 3.5 h. One plausible explanation is the increased average trip length of snapshot distribution $g$, which is about 25% to 30% higher in this period compared to the onset of congestion. Therefore, while fewer trips are generated than completed, the increased average trip length of vehicles present in the network during this time, probably related to rerouting effect in congested conditions, keeps $m/n$ from decreasing. Moreover, fig. 5(b) shows the relation between $m/n$ and accumulation over the simulation time. Interestingly, a counter-clockwise hysteresis loop is observed. For the same accumulation, average remaining distance is higher in the offset of congestion. The explanation is the same as in fig. 5(a): This hysteresis is an inherent property of trip based model when congestion changes over time. Note that this hysteresis loop is not related to the spatial

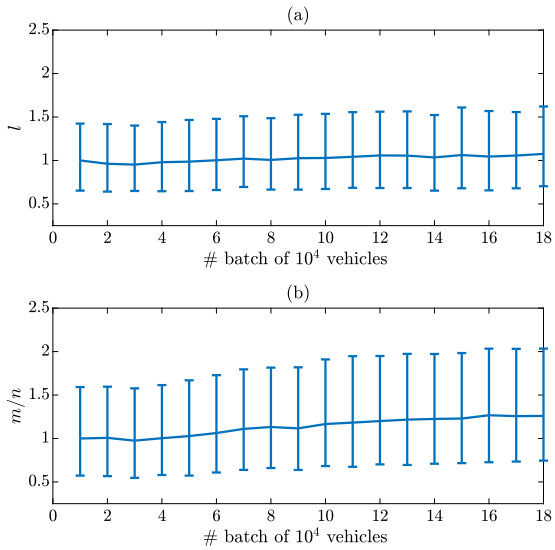


**Fig. 6.** Mean value, 25th and 75th percentiles of (a) generating trip length and (b) average remaining distance to be travelled, for batches of 10 k vehicles in order of departure time. Values are normalized over those of the first batch to highlight evolution over simulation time.

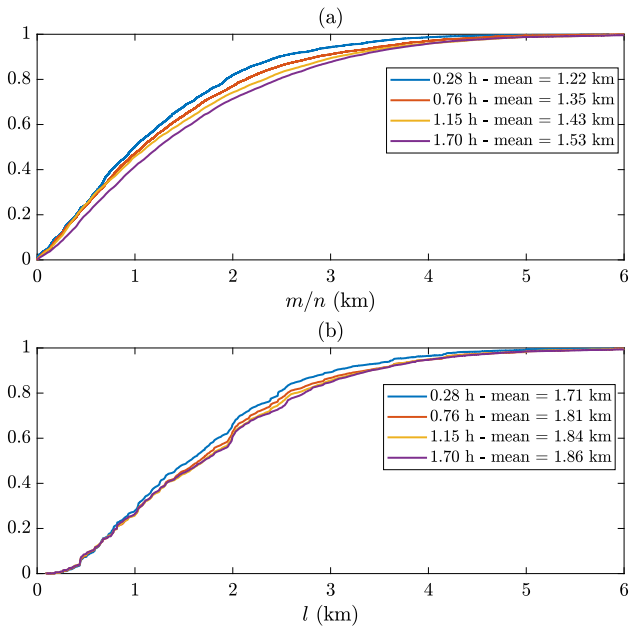


**Fig. 7.** Cumulative distribution functions of (a) remaining distance of individual vehicles and (b) generating trip length distribution, for different times.

distribution of congestion, where more heterogeneous distribution can create lower production or speed for the same accumulation (see for example Geroliminis and Sun (2011a) or Saberi and Mahmassani (2012)). Interestingly, the hysteresis of fig. 5(b) is quite small for values of accumulation larger than the critical accumulation, which is around $1.4 \cdot 10^4$ vehicles.

While these results are consistent with the numerical simulations of an ideal trip based model as presented in Lamotte et al. (2018), assuming a *perfect* speed MFD (i.e., no errors or heterogeneity) and a constant distribution of generating trip length over time, vehicle rerouting and dynamic origin-destination tables might influence the distribution of trip length $f$, and as a result the remaining distance. Thus, we further investigate this in fig. 6, which shows the mean, 25 and 75 percentiles for average trip length $l$ (of the distribution $f$), and the average remaining distance over time. The $x$-axis does not represent equal time intervals, but rather analyzes vehicles in groups of the same size (in batches of $10,000$ vehicles – approximately 5% of the total demand) as they appear in the simulation. While trip length value is unique for each vehicle, remaining distance changes over time. To estimate the distribution of remaining distance we

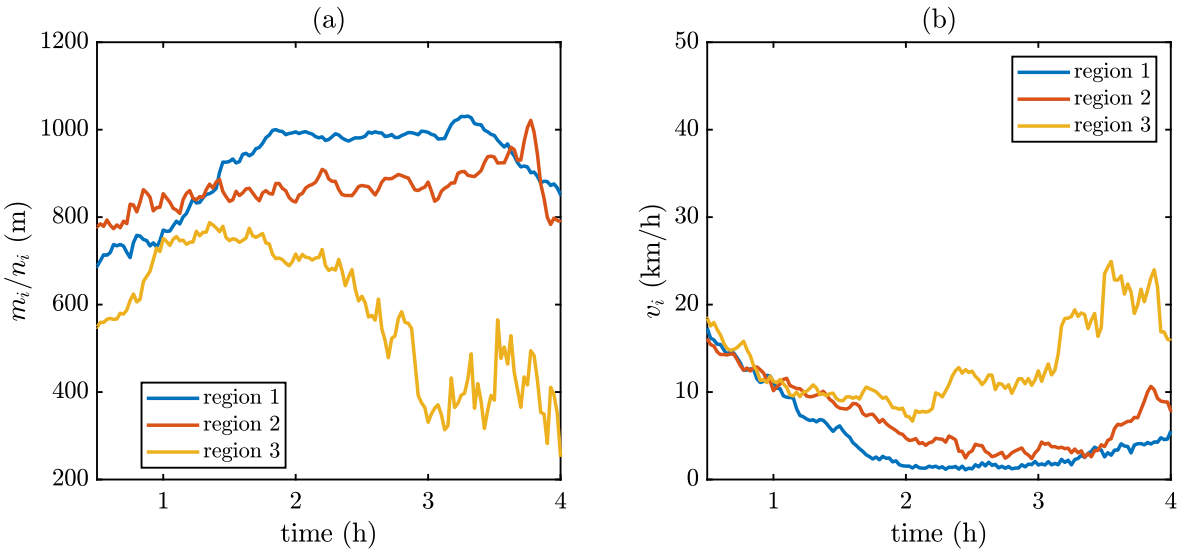


**Fig. 8.** Time series of (a) average remaining distance, and (b) average speed per region ($l_1 = 1192$ m, $l_1^* = 818$ m, $l_2 = 1171$ m, $l_2^* = 888$ m, $l_3 = 852$ m, $l_3^* = 615$ m).

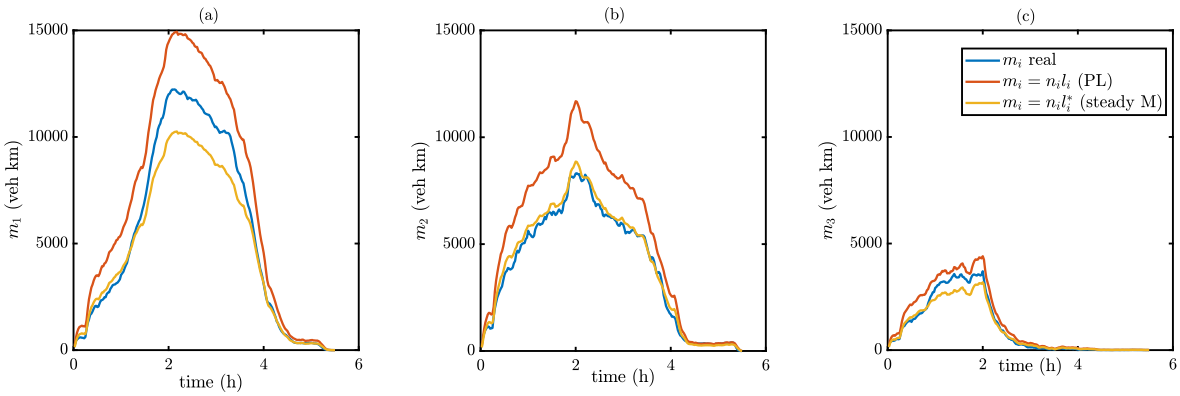


**Fig. 9.** Comparison of $m_i$ observed vs. steady state M model ($m_i = n_i \cdot l_i^*$) vs. PL approximation ($m_i = n_i \cdot l_i$) for each region $i$. The values of average $l_i$ and $l_i^*$ per region are: $l_1 = 1192$ m, $l_1^* = 818$ m, $l_2 = 1171$ m, $l_2^* = 888$ m, $l_3 = 852$ m, $l_3^* = 615$ m.

need to choose a specific time and take a snapshot of the network. For each batch of 10,000 vehicles we take a snapshot the time that the middle vehicle in the batch starts its trip. To perform proper comparisons fig. 6(a) and (b) show dimensionless quantities by dividing all trip length values with the average trip length of the first batch of 10,000 vehicles in the beginning of the simulation (similarly to the average remaining distance estimated in the 1st batch). While $l$ increases slightly during the simulation (not more than 7%), $m/n$ increases following a different trend, reaching even magnitudes of 20%. Note also the higher deviation of the percentiles from the mean for $m/n$. Both $l$ and $m/n$ distributions are skewed to the right during all times and even more during the congested period.

Furthermore, fig. 7 shows the cumulative distribution functions for 4 different time intervals, where $f$ is moderately similar while the remaining distance has a higher degree of variation (mean value $l$ varies around 8% between $t = 0.28$ h and 1.7 h while mean $m/n$ varies about 20% for the same period). These observations highlight that outflow estimates based on a PL model with memoryless characteristics are expected to be more inaccurate compared to an M-model that keeps track of remaining distance to be travelled and would possibly result in better control performance, as it will be shown later in the paper.

Moreover, we are interested in investigating the evolution of $m/n$ over time for individual regions after partitioning. This is shown in fig. 8, where fig. 8(a) shows $m/n$ and fig. 8(b) speed over time, respectively. While the 3 regions have similar speeds in the onset of congestion, as demand increases further regions 1 and 2 experience lower speeds, while region 3 recovers earlier. Nevertheless, average remaining distance follows quite different trends even when speed is equal for the 3 regions (during the first hour of the simulation). These trends are expected to influence the dynamics of accumulations as estimated by the PL and M models. Note for example that the time interval for which $m_i/n_i > l_i^*$ is very different among regions.

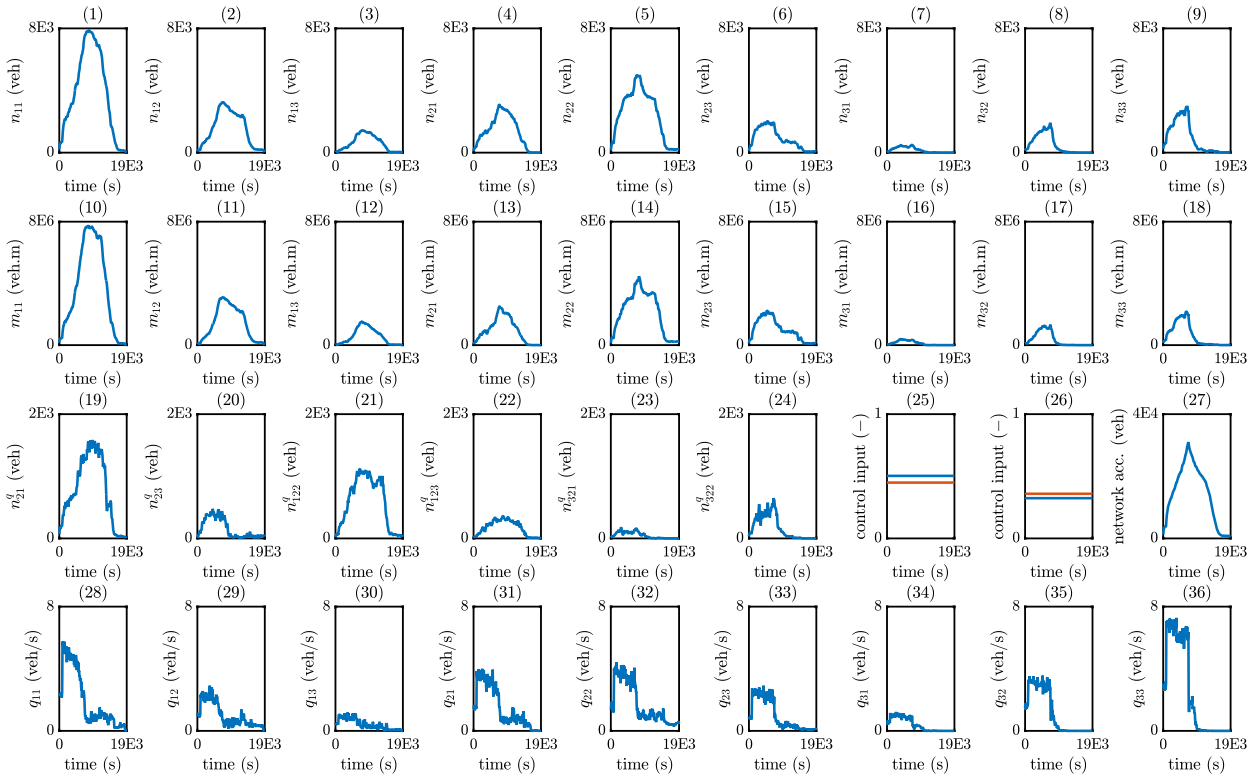


**Fig. 10.** Trajectories of (1)–(9) accumulation states $n_{ij}(k)$, (10)–(18) total remaining distance to be traveled states $m_{ij}(k)$, (19)–(24) boundary queue accumulation states $n^q_{ihj}(k)$, (25) perimeter control inputs $u_{12}(k)$ (blue) and $u_{21}(k)$ (red), (26) perimeter control inputs $u_{23}(k)$ (blue) and $u_{32}(k)$ (red), (27) total network accumulation, and (28)–(36) inflow demands $q_{ij}(k)$, for fixed-time control scenario results via microscopic simulation.

Finally, we estimate the accuracy of the steady state representation of remaining trip distance based on M-model, $m_i = n_i \cdot l_i^*$, and if we assume memoryless conditions of PL model. Given that PL, M and trip based models are identical for exponential trip length distribution (for a proof refer to Lamotte et al. (2018)), remaining distance according to a PL model can be estimated for $l^*$ of an exponential distribution (standard deviation equal to the mean), thus $m_i = n_i \cdot l_i$. Interestingly, fig. 9 shows that the real value of $m_i$ is between the two aforementioned representations, as PL always overestimates $m$ while steady-state M underestimates for region 1 and 3, while it is closer to the real value for region 2. Values of $l_i$ and $l^*$ are given in the caption of the figure. Note that these results are for the whole simulation duration (6 h).

Outflow estimates according to the different models are not provided in this section as they require proper estimation of some parameters of the model. This is described in the next section that contains system identification results and comparison of the models.

### 4.3. Identification results

We consider a congested scenario with fixed-time control (i.e., fixed $u_{ij}(k)$), also referred to as no control scenario, where the network is empty at the beginning and faces increasing inflow demands for some time. Trajectories of state $x(k)$, inflow demand $q(k)$, and control input $u(k)$ are obtained by simulating the scenario for the network in fig. 3 in the microscopic simulation framework Aimsun. The simulation duration is 220 time steps, corresponding to 5.5 hours of real time with a sampling time of $T = 90$ s. Additive white Gaussian noise is added to state trajectory $x(k)$ to emulate presence of sensor noise, yielding the measured state trajectory $x^{\mathrm{m}}(k)$. Results of the microscopic simulation experiment are depicted in fig. 10, showing trajectories of traffic states $n_{ij}, n^q_{ij}$, and $m_{ij}$, alongside control inputs $u_{ih}$ (which are constant due to fixed-time control) and inflow demands $q_{ij}$.

Note that, even after partitioning, the 3 regions experience some significant level of heterogeneity, which is higher during the offset of congestion. While a dynamic partitioning algorithm (see for example Saeedmanesh and Geroliminis (2017)) could decrease the spatial heterogeneity within a region, perimeter control might be more challenging with dynamic zone boundaries and is beyond the scope of this work.

The effect of heterogeneity is captured by the following modification of speed MFDs that models hysteresis (similar to Ramezani et al. (2015)):

$$v_i(n_i(k), \tilde{\sigma}_i(k)) = (a_i \cdot n_i^2(k) + b_i \cdot n_i(k) + c_i) \cdot (d_i \cdot \exp(e_i(\sigma_i(n_i(k)) - \tilde{\sigma}_i(k))) + 1 - d_i), \tag{41}$$

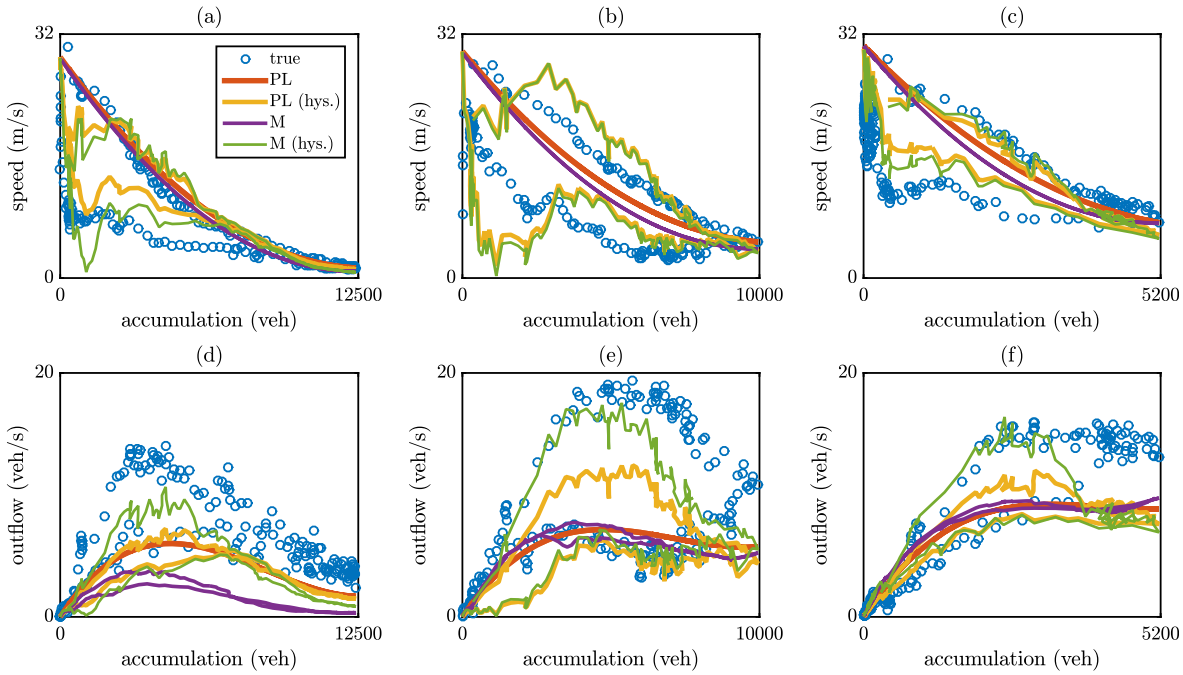


**Fig. 11.** Regional speed (a)-(b)-(c) and outflow (d)-(e)-(f) MFDs showing the true accumulation versus space-mean speed values (blue) and the estimated MFDs with and without hysteresis, for (a)-(d) region 1, (b)-(e) region 2, (c)-(f) region 3, for the no control scenario results via microscopic simulation, comparing the PL and M model-based MBPE.

where $a_i, b_i$, and $c_i$ are MFD parameters, $\widetilde{\sigma}_i(k)$ is the link occupancy standard deviation of region $i$, $d_i$ and $e_i$ are parameters related to heterogeneity effect, whereas $\sigma_i(n_i(k))$ models the link occupancy standard deviation as a function of $n_i(k)$, and is given by:

$$\sigma_i(n_i(k)) = \beta_i n_i^2(k) + \gamma_i n_i(k), \tag{42}$$

where $\beta_i$ and $\gamma_i$ are parameters that can be extracted from historical data $(n_i(k)\text{–}\widetilde{\sigma}_i(k))$, which we computed as follows: $\beta_1 = -3.5624 \cdot 10^{-9}, \gamma_1 = 7.3846 \cdot 10^{-5}, \beta_2 = -4.2255 \cdot 10^{-9}, \gamma_2 = 7.3998 \cdot 10^{-5}, \beta_3 = -1.2688 \cdot 10^{-8}, \gamma_3 = 1.1759 \cdot 10^{-4}$. Note that eq. 41 considers that during the offset of congestion standard deviation of link occupancy is higher, resulting in a negative value inside the exponent and a lower speed. Other functional forms could also be tested by interested readers.

MBPE problem (24) is formulated using direct multiple shooting (Bock and Plitt, 1984), and realized in MATLAB 8.5.0 (R2015a) using the numerical optimal control toolbox CasADi Andersson et al. (2018), with IPOPT Wächter and Biegler (2006) as solver. Given the simulation data, MBPE problem is solved to obtain the parameter vector estimate $\widehat{p}$. The parameter bounds $\underline{p}$ and $\overline{p}$ are chosen in such a way that the MFD parameters are not bounded (since bounding them is seen to lead to computational problems with the MBPE), while $\alpha$ is bounded as $0.01 \leqslant \alpha \leqslant 3.5$ (since in Lamotte et al. (2018) a value of 3 is suggested for $\alpha$, and it is physically meaningful to choose it as positive), while the trip lengths are bounded as $100\text{m} \leqslant l_{ij}^* \leqslant 10000\text{m}$ and $100\text{m} \leqslant l_{ij} \leqslant 10000\text{m}$, considering the dimensions of the road network and choosing relatively loose bounds.

As a result of solving (24), we obtain the estimated speed MFDs and resulting outflow MFD estimates (computed using eq. 1 and eq. 11, respectively, for the PL model and M model cases, and their heterogeneity effect counterparts using eq. 41) shown in fig. 11, together with the following parameter estimates: $\alpha = 1.25$, $a_1 = 1.8376 \cdot 10^{-7}$, $b_1 = -0.0045$, $c_1 = 28.8502$, $d_1 = 4.2147 \cdot 10^3$, $e_1 = 0.0023$, $a_2 = 2.5367 \cdot 10^{-7}$, $b_2 = -0.005$, $c_2 = 29.6686$, $d_2 = 1.293 \cdot 10^4$, $e_2 = 0.0011$, $a_3 = 8.6843 \cdot 10^{-7}$, $b_3 = -0.009$, $c_3 = 30.4754$, $d_3 = 2.5287 \cdot 10^3$, $e_3 = 0.0035$, $l_1 = 7.629 \cdot 10^3$ m, $l_2 = 6.169 \cdot 10^3$ m, $l_3 = 3.599 \cdot 10^3$ m, $l_1^* = 798.4$ m, $l_2^* = 866.9$ m, and $l_3^* = 680.2$. Note that the parameter vector is chosen such that it includes a single parameter $\alpha$ for the whole network, and a pair of parameters $l_i$ and $l_i^*$ for each region $i$. The reason is that through numerical experiments it is found that choices of more parameters (i.e., such as choosing to have one $\alpha$ for each region as $\alpha_i$) lead to problems with identifiability. Future work could include the analysis of model identifiability properties with various parameter vector configurations.

For comparison purposes, the problem (24) can be solved using the PL model in eq. (2), which results in the following parameter estimates: $a_1 = 1.821 \cdot 10^{-7}$, $b_1 = -0.0045$, $c_1 = 28.9795$, $d_1 = 2.5856 \cdot 10^4$, $e_1 = 2.6054 \cdot 10^{-4}$, $a_2 = 2.4336 \cdot 10^{-7}$, $b_2 = -0.0049$, $c_2 = 29.7433$, $d_2 = 2.9518 \cdot 10^4$, $e_2 = 4.6314 \cdot 10^{-4}$, $a_3 = 8.6916 \cdot 10^{-7}$, $b_3 = -0.009$, $c_3 = 30.4963$, $d_3 = 2.907 \cdot 10^4$, $e_3 = 2.4093 \cdot 10^{-4}$, $l_1 = 9.563 \cdot 10^3$ m, $l_2 = 7.921 \cdot 10^3$ m, and $l_3 = 3.821 \cdot 10^3$ m. Note also that as the values of parameters are obtained through an optimization procedure, they might not have an intuitive physical explanation, for example MFD parameters $a_i, b_i$ and $c_i$, or average trip lenghts $l_i$ might be different for M and PL model.

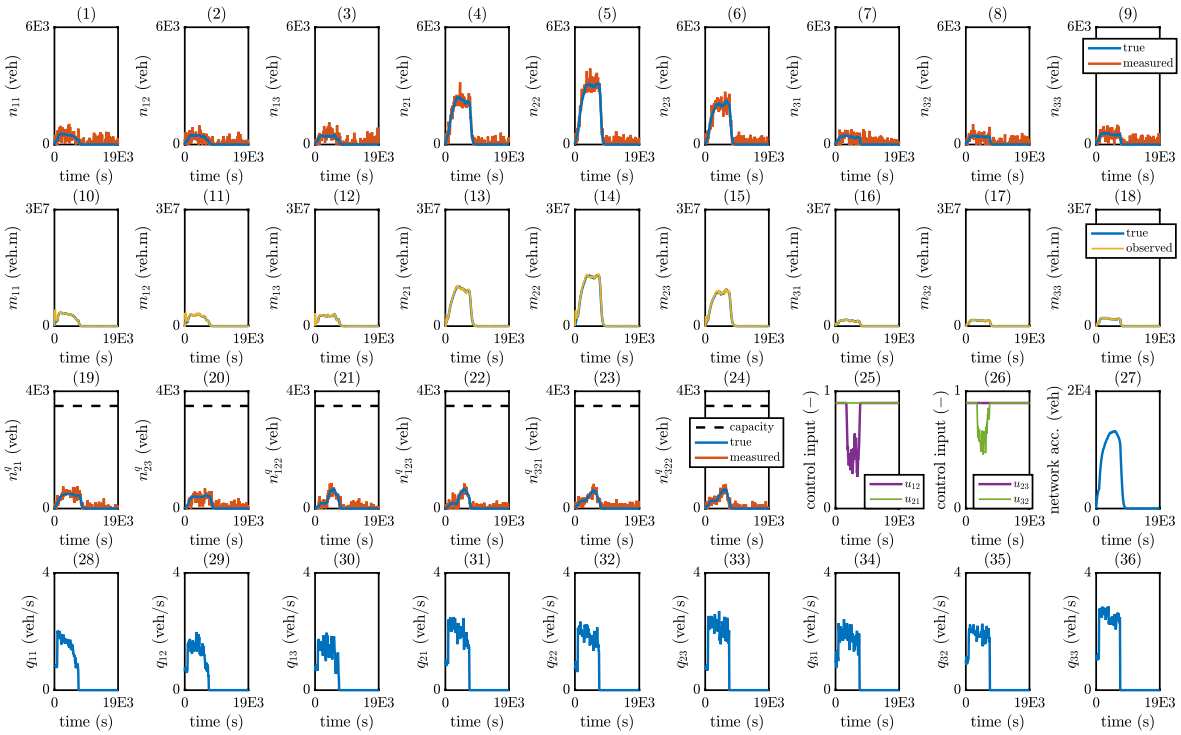


**Fig. 12.** Trajectories of (1)–(9) accumulation states $n_{ij}(k)$, (10)–(18) total remaining distance to be traveled states $m_{ij}(k)$, (19)–(24) boundary queue accumulation states $n^q_{ihj}(k)$, (25) perimeter control inputs $u_{12}(k)$ and $u_{21}(k)$, (26) perimeter control inputs $u_{23}(k)$ and $u_{32}(k)$, (27) total network accumulation, and (28)–(36) inflow demands $q_{ij}(k)$, for the M model-based MHO-MPC scenario results via macroscopic simulation.

The extent to which MBPE method yields accurate outflow estimates for the M-model can be described by the root-mean-square estimation error between the real and estimated outflows:

$$\mathrm{RMSE}_o = \frac{1}{3}\sum_{i=1}^{3}\sqrt{\frac{\sum_{k=1}^{N_{\mathrm{pe}}}\left(o_i(k)-\widetilde{o}_i(k)\right)^2}{N_{\mathrm{pe}}}} \tag{43}$$

where $\widetilde{o}_i(k)$ terms are the estimated outflows, which are considered here since they are common to PL and M models. For the $\widetilde{o}_i(k)$ trajectories obtained by solving MBPE problem (24) using the two models, we obtain $\mathrm{RMSE}_{o,\mathrm{PL}} = 3.63$ veh/s (without heterogeneity modeling, $\mathrm{RMSE}_{o,\mathrm{PL}} = 4.19$ veh/s) and $\mathrm{RMSE}_{o,\mathrm{M}} = 3.01$ veh/s (without heterogeneity modeling, $\mathrm{RMSE}_{o,\mathrm{M}} = 4.83$ veh/s). These results indicate that consideration of heterogeneity modeling achieves a better fit between the estimated and true states, suggesting that heterogeneity can capture more accurately detailed traffic dynamics. Furthermore, from the outflows RMSE values and fig. 11 it can be seen that M-model can yield more realistic estimates of regional space-mean speed and outflow values, compared to PL model, as indicated by the better match between true and estimated values. These results suggest that M-model has the potential of reproducing large-scale traffic dynamics more accurately than the PL model.

Note that there is a substantial difference between the parameter values obtained from Aimsun and those identified by the MBPE problem. For example, the average trip length for region 1 is obtained as $l_1 = 1192$ m, while the MBPE finds the same value as $l_1 = 7629$ m. Our simulation studies on this issue (which we omit here for brevity) provide us with numerical evidence that this can be mainly attributed to plant-model mismatch, i.e., the difference between the dynamics in Aimsun and the M-model. Roughly stated, the difference in parameter values can be understood as the way in which MBPE compensates for the plant-model mismatch. This issue needs more research effort for a complete understanding, and there can be further questions such as how the control performance would change according to the parameter value in the MPC prediction model. We consider these interesting directions for future work.

### 4.4. Control results

The model parameters vector $\widehat{p}$ obtained by the M-model-based MBPE method (without heterogeneity effect) is used to build a simulator based on the M-model dynamics, and used in the MHO and MPC schemes to control the urban network via perimeter control actuation for improving mobility under situations with noisy measurements. For comparison purposes, a PL model-based MPC scheme is also constructed, which uses the model parameters vector $\widehat{p}$) obtained by the PL model-based MBPE method (without heterogeneity

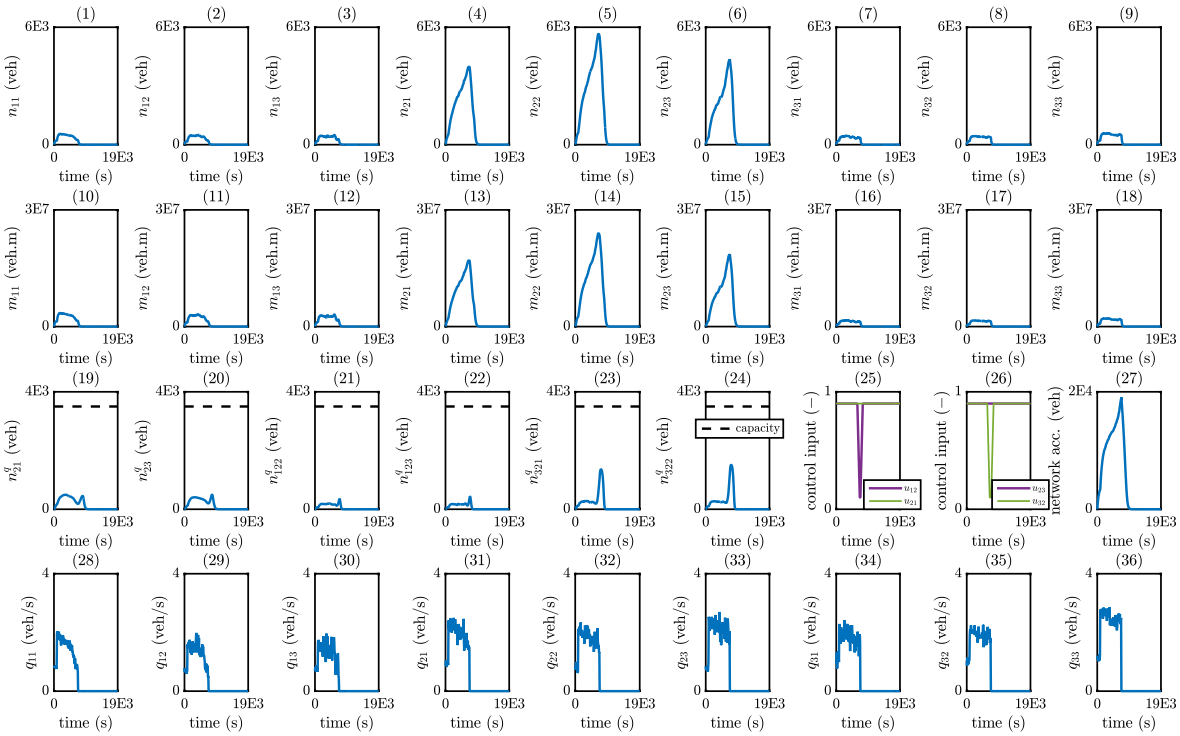


**Fig. 13.** Trajectories of (1)–(9) accumulation states $n_{ij}(k)$, (10)–(18) total remaining distance to be traveled states $m_{ij}(k)$, (19)–(24) boundary queue accumulation states $n^q_{ihj}(k)$, (25) perimeter control inputs $u_{12}(k)$ and $u_{21}(k)$, (26) perimeter control inputs $u_{23}(k)$ and $u_{32}(k)$, (27) total network accumulation, and (28)–(36) inflow demands $q_{ij}(k)$, for the PL model-based MPC scenario results via macroscopic simulation.

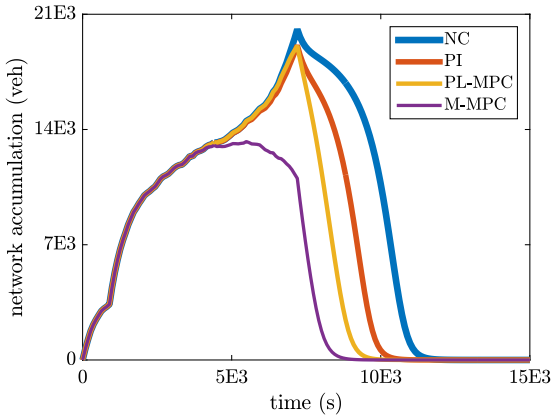


**Fig. 14.** Trajectories of total network accumulation (i.e., sum of all $n_{ij}$ and $n^q_{ihj}$ states, for no control case, the PI controller, the PL model- and M-based MPC schemes.

effect). The MHO and MPC schemes are built using direct multiple shooting (Bock and Plitt, 1984), and realized in MATLAB 8.5.0 (R2015a) using the numerical optimal control toolbox CasADi (Andersson et al., 2018), with IPOPT (Wächter and Biegler, 2006) as solver, while the dynamics are discretized with the Runge–Kutta (RK4) method with a sampling time of 90 s to reflect a realistic number for traffic light cycle length. Observation and prediction horizons are chosen as $N_o = 20$ and $N_c = 30$, respectively. Simulation duration is $K = 220$ in number of time-steps, corresponding to 5.5 h of real time. The simulation operates by evolving traffic conditions through a macroscopic simulator that is realized by creating a numerical integrator using the M-model dynamics eq. (19), where MHO-MPC code is executed every 90 s (i.e., the operation outlined in algorithm 1 is simulated).

Results of the macroscopic simulation experiments with control are depicted in fig. 12 (with M-model-based MHO-MPC) and fig. 13 (with PL model-based MPC), showing trajectories of traffic states $n_ij, n^q_{ij}$, and $m_{ij}$ (for M-model-based MHO-MPC, showing true trajectories and those observed by MHO), alongside control inputs $u_{ih}$ and inflow demands $q_{ij}$; finally, fig. 14 shows the total network

accumulation for the no control case (i.e., constant $u_{ih}$) and the two MPC schemes (also including a simple PI controller trying to keep the central region at capacity). From the accumulation trajectories it can be seen that the M-model-based MHO-MPC scheme yields lower accumulation values compared to PL model-based MPC scheme. Moreover, it can be seen from $m_{ij}$ trajectories for the M-model-based MHO-MPC scheme that MHO is capable of reconstructing the $m_{ij}$ states accurately without having any $m_{ij}$ measurements. We also note that buffer zone accumulations never exceed storage capacity that could create overflow issues in the modeling. Another observation is that control actions are quite different with M-model-based MPC scheme and remain for a shorter duration at the minimum values. M controller is activated earlier than the PL controller and before regions reach their critical accumulation. While this has no effect in the total accumulation until time $5 \cdot 10^3$ sec (as seen in fig. 14), it significantly improves system delays afterwards.

The total time spent in the network is $1.34 \cdot 10^8$ veh.s for no control, $1.22 \cdot 10^8$ veh.s for PI controller, $1 \cdot 10^8$ veh.s for the PL-model based MPC, and $7.9 \cdot 10^7$ veh.s for M-model based MPC, indicating that M-model based MPC can improve mobility by 41% compared to no control, 30% compared to PI controller, and 21% compared to the PL-model based MPC. Overall, these results suggest that M-model based MHO-MPC scheme carries potential for improved performance in large-scale traffic control, by utilizing the remaining travel distance dynamics in the prediction models. Moreover, the CPU times of the MHO algorithm are 0.47 s (mean) and 0.57 s (maximum), while those of the M-model based MPC are 1.33 s (mean) and 2.56 s (maximum), which are negligible with respect to the sampling time of 90 s, indicating the real-time feasibility of the proposed methods.

## 5. Conclusion

In this paper we developed a multi-region extension for the M-model that captures the effects of remaining travel distance dynamics on large-scale traffic flows. We also developed a system identification (SI) method for the multi-region M-model with boundary queues. As M-model contains one additional parameter that has a mathematical meaning rather than a physical one (how much the outflow deviates from the steady state), a rigorous SI method is considered to appropriately handle the challenges associated with the model. We proposed a nonlinear moving horizon observer for the M-model that can reconstruct total remaining distance to be traveled states $m_{ij}$ by exclusively using accumulation state measurements, which is intended for enabling M-model-based control where the full state including $m_{ij}$ is not available. An economic nonlinear MPC formulation is given using M-model for improving mobility in large-scale urban networks via perimeter control actuation. Microscopic simulations are used for generating data to be used for the SI method in estimating M-model parameters vector, which is then used in macroscopic simulations, demonstrating the operation of the M-model-based observer and control schemes. Results indicate the potential of M-model in capturing detailed traffic dynamics and thus achieving higher performance in model-based large-scale traffic control. Future work could investigate different combinations of monitoring techniques and estimation methods for directly estimating remaining distance variables $m_{ij}$. A combination of loop detectors and sample of vehicle trajectories could serve this objective. This could also allow for a direct comparison of PL and M-model based MPC controls in a micro-simulation environment. A comparison of the results of Section 4.4 for a PL model with buffer zones (similar to Ni and Cassidy (2019)) could also shed more light in the performance of different controllers. Investigating the performance of M-model with real data should also be another research direction. Furthermore, dynamic trip lengths can be considered in the models, requiring them to be either measured or observed. Measuring trip lengths in real-time is expected to be difficult (and thus problematic from the practice point of view), while there could be complications related to observability, i.e., it may not be mathematically possible to extract dynamically varying trip lengths from standard measurements such as the accumulations. Considering dynamic trip lengths in the modeling, estimation, and control formulations is thus another possible direction for future work.

## CRediT authorship contribution statement

**Isik Ilber Sirmatel:** Conceptualization, Methodology, Investigation, Validation, Writing - review & editing, Formal analysis, Visualization, Software, Writing - original draft. **Dimitrios Tsitsokas:** Conceptualization, Methodology, Investigation, Validation, Writing - review & editing, Formal analysis, Visualization, Software. **Anastasios Kouvelas:** Conceptualization, Methodology, Investigation, Validation, Writing - review & editing, Formal analysis, Visualization, Software, Supervision. **Nikolas Geroliminis:** Conceptualization, Methodology, Investigation, Validation, Writing - review & editing, Writing - original draft, Supervision.

## Acknowledgements

I.I.S. is supported by the Swiss National Science Foundation (SNSF) under the National Centre of Competence in Research, Dependable Ubiquitous Automation (NCCR Automation), grant agreement 51NF40_180545. D.T. is supported by the Swiss National Science Foundation (SNSF) under the project name DIPLOMAT, contract No. 205121-165644. The authors are grateful to Dr. Mikhail Murashkin and Dr. Raphaël Lamotte from Urban Transport Systems Lab (LUTS, EPFL) for fruitful discussions in the early stages of this work.

## References

Aalipour, A., Kebriaei, H., Ramezani, M., 2019. Analytical optimal solution of perimeter traffic flow control based on MFD dynamics: A Pontryagin's maximum principle approach. IEEE Trans. Intell. Transp. Syst. 20, 3224–3234. https://doi.org/10.1109/TITS.2018.2873104.

Aboudolas, K., Geroliminis, N., 2013. Perimeter and boundary flow control in multi-reservoir heterogeneous networks. Transp. Res. Part B: Methodol. 55, 265–281. https://doi.org/10.1016/j.trb.2013.07.003.

Andersson, J.A., Gillis, J., Horn, G., Rawlings, J.B., Diehl, M., 2018. CasADi: A software framework for nonlinear optimization and optimal control. Math. Program. Comput. 1–36 https://doi.org/10.1007/s12532-018-0139-4.
Arnott, R., 2013. A bathtub model of downtown traffic congestion. J. Urban Econ. 76, 110–121. https://doi.org/10.1016/j.jue.2013.01.001.
Besançon, G., 2007. An overview on observer tools for nonlinear systems. In: Nonlinear observers and applications. Springer, pp. 1–33.
Bock, H.G., Körkel, S., Schlöder, J.P., 2013. Parameter estimation and optimum experimental design for differential equation models. In: Model based parameter estimation. Springer, pp. 1–30.
Bock, H.G., Plitt, K.J., 1984. A multiple shooting algorithm for direct solution of optimal control problems. In: IFAC Proceedings. 9th IFAC World Congress: A Bridge Between Control Science and Technology, Budapest, Hungary, 2-6 July 1984, vol. 17, pp. 1603–1608. doi: 10.1016/S1474-6670(17)61205-9.
Buisson, C., Ladier, C., 2009. Exploring the impact of homogeneity of traffic measurements on the existence of macroscopic fundamental diagrams. Transp. Res. Rec.: J. Transp. Res. Board 2124, 127–136. https://doi.org/10.3141/2124-12.
Csikós, A., Charalambous, T., Farhadi, H., Kulcsár, B., Wymeersch, H., 2017. Network traffic flow optimization under performance constraints. Transp. Res. Part C: Emerg. Technol. 83, 120–133. https://doi.org/10.1016/j.trc.2017.08.002.
Daganzo, C.F., 2007. Urban gridlock: Macroscopic modeling and mitigation approaches. Transp. Res. Part B: Methodol. 41, 49–62. https://doi.org/10.1016/j.trb.2006.03.001.
Daganzo, C.F., Lehe, L.J., 2015. Distance-dependent congestion pricing for downtown zones. Transp. Res. Part B: Methodol. 75, 89–99. https://doi.org/10.1016/j.trb.2015.02.010.
Ding, H., Guo, F., Zheng, X., Zhang, W., 2017. Traffic guidance–perimeter control coupled method for the congestion in a macro network. Transp. Res. Part C: Emerg. Technol. 81, 300–316. https://doi.org/10.1016/j.trc.2017.06.010.
Fosgerau, M., 2015. Congestion in the bathtub. Econ. Transp. 4, 241–255. https://doi.org/10.1016/j.ecotra.2015.08.001.
Geroliminis, N., Daganzo, C.F., 2008. Existence of urban-scale macroscopic fundamental diagrams: Some experimental findings. Transp. Res. Part B: Methodol. 42, 759–770. https://doi.org/10.1016/j.trb.2008.02.002.
Geroliminis, N., Haddad, J., Ramezani, M., 2013. Optimal perimeter control for two urban regions with macroscopic fundamental diagrams: A model predictive approach. IEEE Trans. Intell. Transp. Syst. 14, 348–359. https://doi.org/10.1109/TITS.2012.2216877.
Geroliminis, N., Sun, J., 2011a. Hysteresis phenomena of a macroscopic fundamental diagram in freeway networks. Transp. Res. Part A: Policy Pract. 45, 966–979. https://doi.org/10.1016/j.tra.2011.04.004.
Geroliminis, N., Sun, J., 2011b. Properties of a well-defined macroscopic fundamental diagram for urban traffic. Transp. Res. Part B: Methodol. 45, 605–617. https://doi.org/10.1016/j.trb.2010.11.004.
Godfrey, J., 1969. The mechanism of a road network. Traff. Eng. Control 8.
Guo, Q., Ban, X.J., 2020. Macroscopic fundamental diagram based perimeter control considering dynamic user equilibrium. Transp. Res. Part B: Methodol. 136, 87–109. https://doi.org/10.1016/j.trb.2020.03.004.
Haddad, J., 2017a. Optimal coupled and decoupled perimeter control in one-region cities. Control Eng. Pract. 61, 134–148. https://doi.org/10.1016/j.conengprac.2017.01.010.
Haddad, J., 2017b. Optimal perimeter control synthesis for two urban regions with aggregate boundary queue dynamics. Transp. Res. Part B: Methodol. 96, 1–25. https://doi.org/10.1016/j.trb.2016.10.016.
Haddad, J., Geroliminis, N., 2012. On the stability of traffic perimeter control in two-region urban cities. Transp. Res. Part B: Methodol. 46, 1159–1176. https://doi.org/10.1016/j.trb.2012.04.004.
Haddad, J., Mirkin, B., 2016. Adaptive perimeter traffic control of urban road networks based on mfd model with time delays. Int. J. Robust Nonlinear Control 26, 1267–1285. https://doi.org/10.1002/rnc.3502.
Haddad, J., Mirkin, B., 2017. Coordinated distributed adaptive perimeter control for large-scale urban road networks. Transp. Res. Part C: Emerg. Technol. 77, 495–515. https://doi.org/10.1016/j.trc.2016.12.002.
Haddad, J., Mirkin, B., 2020. Resilient perimeter control of macroscopic fundamental diagram networks under cyberattacks. Transp. Res. Part B: Methodol. 132, 44–59. https://doi.org/10.1016/j.trb.2019.01.020.
Haddad, J., Shraiber, A., 2014. Robust perimeter control design for an urban region. Transp. Res. Part B: Methodol. 68, 315–332. https://doi.org/10.1016/j.trb.2014.06.010.
Haddad, J., Zheng, Z., 2020. Adaptive perimeter control for multi-region accumulation-based models with state delays. Transp. Res. Part B: Methodol. 137, 133–153. https://doi.org/10.1016/j.trb.2018.05.019.
Hajiahmadi, M., Haddad, J., De Schutter, B., Geroliminis, N., 2015. Optimal hybrid perimeter and switching plans control for urban traffic networks. IEEE Trans. Control Syst. Technol. 23, 464–478. https://doi.org/10.1109/TCST.2014.2330997.
Ingole, D., Mariotte, G., Leclercq, L., 2020. Perimeter gating control and citywide dynamic user equilibrium: A macroscopic modeling framework. Transp. Res. Part C: Emerg. Technol. 111, 22–49. https://doi.org/10.1016/j.trc.2019.11.016.
Jin, W.L., 2020. Generalized bathtub model of network trip flows. Transp. Res. Part B: Methodol. 136, 138–157. https://doi.org/10.1016/j.trb.2020.04.002.
Keyvan-Ekbatani, M., Kouvelas, A., Papamichail, I., Papageorgiou, M., 2012. Exploiting the fundamental diagram of urban networks for feedback-based gating. Transp. Res. Part B: Methodol. 46, 1393–1403. https://doi.org/10.1016/j.trb.2012.06.008.
Kouvelas, A., Saeedmanesh, M., Geroliminis, N., 2017. Enhancing model-based feedback perimeter control with data-driven online adaptive optimization. Transp. Res. Part B: Methodol. 96, 26–45. https://doi.org/10.1016/j.trb.2016.10.011.
Lamotte, R., Geroliminis, N., 2016. The morning commute in urban areas: Insights from theory and simulation. In: Transportation Research Board 95th Annual Meeting. URL: https://trid.trb.org/view/1392730.
Lamotte, R., Geroliminis, N., 2018. The morning commute in urban areas with heterogeneous trip lengths. Transp. Res. Part B: Methodol. 117, 794–810. https://doi.org/10.1016/j.trb.2017.08.023.
Lamotte, R., Murashkin, M., Kouvelas, A., Geroliminis, N., 2018. Dynamic modeling of trip completion rate in urban areas with MFD representations. In: Transportation Research Board 97th Annual Meeting. URL: https://trid.trb.org/view/1497158.
Lei, T., Hou, Z., Ren, Y., 2020. Data-driven model free adaptive perimeter control for multi-region urban traffic networks with route choice. IEEE Trans. Intell. Transp. Syst. 21, 2894–2905. https://doi.org/10.1109/TITS.2019.2921381.
Ljung, L., 2002. Prediction error estimation methods. Circ. Syst. Sig. Process. 21, 11–21. https://doi.org/10.1007/BF01211648.
Mahmassani, H.S., Williams, J.C., Herman, R., 1984. Investigation of network-level traffic flow relationships: Some simulation results. Transp. Res. Rec. 971, 121–130.
Mariotte, G., Leclercq, L., Laval, J.A., 2017. Macroscopic urban dynamics: Analytical and numerical comparisons of existing models. Transp. Res. Part B: Methodol. 101, 245–267. https://doi.org/10.1016/j.trb.2017.04.002.
Menelaou, C., Kolios, P., Timotheou, S., Panayiotou, C., Polycarpou, M., 2017. Controlling road congestion via a low-complexity route reservation approach. Transp. Res. Part C: Emerg. Technol. 81, 118–136. https://doi.org/10.1016/j.trc.2017.05.005.
Michalska, H., Mayne, D.Q., 1995. Moving horizon observers and observer-based control. IEEE Trans. Autom. Control 40, 995–1006. https://doi.org/10.1109/9.388677.
Mohajerpoor, R., Saberi, M., Vu, H.L., Garoni, T.M., Ramezani, M., 2020. H-inf robust perimeter flow control in urban networks with partial information feedback. Transp. Res. Part B: Methodol. 137, 47–73.
Ni, W., Cassidy, M., 2019. City-wide traffic control: Modeling impacts of cordon queues. Transp. Res. Part C: Emerg. Technol. https://doi.org/10.1016/j.trc.2019.04.024.
Papamichail, I., Papageorgiou, M., 2010. Balancing of queues or waiting times on metered dual-branch on-ramps. IEEE Trans. Intell. Transp. Syst. 12, 438–452. https://doi.org/10.1109/TITS.2010.2093130.

Ramezani, M., Haddad, J., Geroliminis, N., 2015. Dynamics of heterogeneity in urban networks: Aggregated traffic modeling and hierarchical control. Transp. Res. Part B: Methodol. 74, 1–19. https://doi.org/10.1016/j.trb.2014.12.010.

Ramezani, M., Nourinejad, M., 2018. Dynamic modeling and control of taxi services in large-scale urban networks: A macroscopic approach. Transp. Res. Part C: Emerg. Technol. 94, 203–219. https://doi.org/10.1016/j.trc.2017.08.011.

Ren, Y., Hou, Z., Sirmatel, I.I., Geroliminis, N., 2020. Data driven model free adaptive iterative learning perimeter control for large-scale urban road networks. Transp. Res. Part C: Emerg. Technol. 115, 102618. https://doi.org/10.1016/j.trc.2020.102618.

Saberi, M., Mahmassani, H.S., 2012. Exploring properties of networkwide flow–density relations in a freeway network. Transp. Res. Rec.: J. Transp. Res. Board 2315, 153–163. https://doi.org/10.3141/2315-16.

Saeedmanesh, M., Geroliminis, N., 2016. Clustering of heterogeneous networks with directional flows based on "Snake" similarities. Transp. Res. Part B: Methodol. 91, 250–269. https://doi.org/10.1016/j.trb.2016.05.008.

Saeedmanesh, M., Geroliminis, N., 2017. Dynamic clustering and propagation of congestion in heterogeneously congested urban traffic networks. Transp. Res. Part B: Methodol. 105, 193–211. https://doi.org/10.1016/j.trb.2017.08.021.

Sirmatel, I.I., Geroliminis, N., 2018. Economic model predictive control of large-scale urban road networks via perimeter control and regional route guidance. IEEE Trans. Intell. Transp. Syst. 19, 1112–1121. https://doi.org/10.1109/TITS.2017.2716541.

Sirmatel, I.I., Geroliminis, N., 2019. Nonlinear moving horizon estimation for large-scale urban road networks. IEEE Trans. Intell. Transp. Syst. https://doi.org/10.1109/TITS.2019.2946324.

Sirmatel, I.I., Geroliminis, N., 2020. Model-based identification, estimation, and control for large-scale urban road networks. In: 2020 European Control Conference (ECC). IEEE, pp. 408–413. https://doi.org/10.23919/ECC51009.2020.9143995.

Su, Z., Chow, A.H., Zheng, N., Huang, Y., Liang, E., Zhong, R., 2020. Neuro-dynamic programming for optimal control of macroscopic fundamental diagram systems. Transp. Res. Part C: Emerg. Technol. 116, 102628. https://doi.org/10.1016/j.trc.2020.102628.

Wächter, A., Biegler, L.T., 2006. On the implementation of an interior-point filter line-search algorithm for large-scale nonlinear programming. Math. Program. 106, 25–57. https://doi.org/10.1007/s10107-004-0559-y.

Yildirimoglu, M., Ramezani, M., 2020. Demand management with limited cooperation among travellers: A doubly dynamic approach. Transp. Res. Part B: Methodol. 132, 267–284. https://doi.org/10.1016/j.trb.2019.02.012.

Yildirimoglu, M., Sirmatel, I.I., Geroliminis, N., 2018. Hierarchical control of heterogeneous large-scale urban road networks via path assignment and regional route guidance. Transp. Res. Part B: Methodol. 118, 106–123. https://doi.org/10.1016/j.trb.2018.10.007.

Zhong, R., Chen, C., Huang, Y., Sumalee, A., Lam, W., Xu, D., 2018. Robust perimeter control for two urban regions with macroscopic fundamental diagrams: A control-lyapunov function approach. Transp. Res. Part B: Methodol. 117, 687–707. https://doi.org/10.1016/j.trb.2017.09.008.

Zhou, Z., De Schutter, B., Lin, S., Xi, Y., 2017. Two-level hierarchical model-based predictive control for large-scale urban traffic networks. IEEE Trans. Control Syst. Technol. 25, 496–508. https://doi.org/10.1109/TCST.2016.2572169.